Giaralis A. An inerter-based dynamic vibration absorber with concurrently enhanced energy harvesting and motion control performances under broadband stochastic excitation via inertance amplification. *ASCE-ASME Journal of Risk and Uncertainty in Engineering Systems Part B: Mechanical Engineering, accepted*: 16/11/2020.

An inerter-based dynamic vibration absorber with concurrently enhanced energy harvesting and motion control performances under broadband stochastic excitation via inertance amplification

Agathoklis Giaralis

School of Mathematics, Computer Science and Engineering,
City, University of London
Northampton Square, London EC1V 0HB, UK

Abstract

This paper examines the performance of a regenerative dynamic vibration absorber, dubbed energy harvesting-enabled tuned mass-damper-inerter (EH-TMDI), for simultaneous vibration suppression and energy harvesting in white noise excited damped linear primary structures. Single-degree-of-freedom (SDOF) structures under force and base excitations are studied as well as multi-degree-of-freedom (MDOF) structures under correlated random forces. The EH-TMDI includes an electromagnetic motor (EM), assumed to behave as a shunt damper, sandwiched between a secondary mass and an inerter element connected in series. The latter element resists relative acceleration at its ends through a constant termed inertance known to be readily scalable in actual inerter device implementations. In this regard, attention is herein focused on gauging the available energy for harvesting at the EM and the displacement variance of the primary structure as the inertance increases through comprehensive parametric investigations. This is supported by adopting simplified inertance-dependent tuning formulae for the EH-TMDI stiffness and damping properties and deriving in closed-form the response of white-noise excited EH-TMDI-equipped SDOF and MDOF systems through linear random vibration analyses. It is found that lightweight EH-TMDIs, having 1% the mass of the primary structure, achieve improved vibration suppression *and* energy harvesting performance as inertance amplifies. For SDOF structures with grounded inerter, the rate of improvement is higher as the inherent structural damping reduces and the EM shunt damping increases. For MDOF structures with non-grounded inerter, improvement rate is higher as the primary structure flexibility between the two EH-TMDI attachment points increases.

Keywords: Tuned mass damper inerter (TMDI); shunt damping; energy harvesting; vibration control; correlated random excitation; inertance.

1. Introduction

Passive dynamic vibration absorbers (DVAs), with most representative the linear tuned mass damper (TMD) (Den Hartog 1956), have found widespread application for suppressing the motion of dynamically excited (primary) structures and structural components (e.g., Elias and Matsagar 2017). In its simplest form, the TMD consists of a free-to-vibrate (secondary) mass attached to the primary structure through spring (stiffness) and dashpot (damping) elements. Motion suppression is achieved by transferring kinetic energy from the primary structure to the secondary mass, which is eventually dissipated by the damping element. This is facilitated by tuning the TMD stiffness, for a given TMD

Giaralis A. An inerter-based dynamic vibration absorber with concurrently enhanced energy harvesting and motion control performances under broadband stochastic excitation via inertance amplification. *ASCE-ASME Journal of Risk and Uncertainty in Engineering Systems Part B: Mechanical Engineering, accepted*: 16/11/2020.

secondary mass, to the dominant natural frequency of the primary structure and by providing sufficient TMD damping for efficient energy dissipation (e.g., Warburton 1982). Commonly, damping is provided by linear viscous dampers, in which case the dissipated kinetic energy becomes heat (e.g., Lee and Taylor 2001). Alternatively, damping may be supplied to TMDs, or more generally to DVAs, by electromagnetic motors (EMs) (e.g., Palomera-Arias et al. 2008, Zhu et al. 2012), or piezo-electric material (e.g., Adhikari et al. 2009) coupled with power electronics energy harvesting and storage circuitry. In the latter case, DVAs become dynamic energy harvesters, also termed regenerative DVAs, which transform the kinetic energy of the primary structure into usable electricity (e.g., Tang and Zuo 2012, Zuo and Tang 2013, Shen et al. 2018). In this setting, regenerative TMDs can serve the dual purpose of energy harvesting and vibration suppression and significant research has been devoted to reconcile these two objectives for different types of primary structures and excitations (e.g., Zuo and Cui 2013, Gonzalez-Buelga *et al.* 2014, Shen *et al.* 2019).

In recent years, inerter components have been considered to improve the motion suppression performance of TMDs (e.g., Lazar et al. 2014, Marian and Giaralis 2014) as well as to enhance the energy harvesting potential of EMs (e.g., Cassidy *et al.* 2011, Green et al. 2015, Zhu et al. 2019) and of regenerative DVAs (e.g., Salvi and Giaralis 2016, Marian and Giaralis 2017, Joubaneh and Barry 2019). Theoretically, the ideal inerter is defined as a massless linear mechanical element which resists relative acceleration through a constant of proportionality, dubbed "inertance" and measured in mass units (kg) (Smith 2002). Technologically, inerter embodiments with inertance several orders of magnitude higher than the device physical mass have been prototyped and experimentally verified (Smith 2020). This has been widely achieved by considering mechanisms transforming the translational motion of the device ends into rotational motion of a lightweight fast-spinning disk (flywheel) (Papageorgiou and Smith 2005, Wang et al. 2011, Pietrosanti et al. 2020), among other alternatives (Swift et al. 2013, Gonzalez-Buelga et al. 2015, Liu et al. 2018). In this respect, inertance scalability has been leveraged to define various lightweight DVA configurations (see Taflanidis et al. 2019 and therein references), including the tuned mass damper inerter (TMDI) (Marian and Giaralis 2014), in which the inerter acts as mass amplifier to the secondary mass, and the tuned inerter damper (TID) (Lazar et al. 2014), in which the inerter replaces the secondary mass. In fact, the TMDI/TID were shown to achieve better vibration suppression performance than the TMD as inertance increases for randomly excited primary structures modelled as single degree of freedom (SDOF) systems (e.g., De Angelis et al. 2019), as well as lumped-mass multi degree of freedom (MDOF) systems (e.g., Marian and Giaralis 2014, Giaralis and Petrini 2017). Further, the TMDI/TID were shown to be more robust than the TMD to detuning effects due to uncertainty in the properties of the primary structure as well as the random excitation (Giaralis and Taflanidis 2018). Independently from the above developments, inerter-like mechanisms have been embedded within rotational EMs to increase energy generation potential from large-amplitude, low-frequency vibrations by acting as motion amplifiers (Cassidy et al. 2011, Green et al. 2015, Zhu et al. 2019). Such rotational EMs find wide application in regenerative DVAs (Tang and Zuo 2012, Shen et al. 2018). Moreover, standalone inerter devices have been also considered to improve the vibration suppression and/or energy generation performances of regenerative DVAs as the introduced inertance increases (Salvi and Giaralis 2016, Marian and Giaralis 2017, Joubaneh and Barry 2019, Petrini et al. 2020).

To this end, of particular importance to this work is to recognize that the inertance of typical inerter device implementations can readily magnify. One way to accomplish this is by increasing the mass

moment of inertia of the flywheel. For instance, Hu et al. (2016) prototyped a circular flywheel with attached sliding masses whose distance from the center of the flywheel are adjusted via a servo-electric mechanism to achieve a semi-active inerter with real-time varying/increasing inertance. Further, Pietrosanti et al (2020) built an inerter with a modular flywheel whose mass can readily change off-line to facilitate parametric experimental testing. Alternatively, Brzeski et al. (2017) demonstrated experimentally the feasibility of inerter devices which can achieve any desired intermediate inertance value on-the-fly by using a continuously varying transmission to drive the flywheel (see also Lazarek et al. 2019). The thus demonstrated technological readiness of inerter devices with varying inertance has recently prompted the investigation of the performance of regenerative inerter-based DVAs under increasing inertance. In this regard, Marian and Giaralis (2017) studied numerically the performance of a regenerative TMDI configuration for vibration suppression and energy harvesting from harmonically excited SDOF systems. The considered configuration featured an inerter connecting the secondary mass to the ground such that inertance was added directly to the inertia of the DVA, while an EM was used to attach the secondary mass to the primary structure. It was found that the available energy for harvesting increased with increasing inertance but at the expense of poorer vibration suppression performance. Similar trends were also reported in a study by Petrini et al. (2020) who considered a regenerative TMDI with non-grounded inerter attached to the lead mass of a lumped-mass cantilevered MDOF primary structure under correlated random excitation. Nevertheless, Salvi and Giaralis (2016) considered a variant regenerative inerter-based DVA and demonstrated, through a numerical parametric investigation, concurrent improvement of energy harvesting and vibration suppression performances with increasing inertance in SDOF primary structures under resonant harmonic excitation. In the latter DVA, termed energy-harvesting enabled TMDI (EH-TMDI), the EM was placed in series in between the secondary mass and a grounded inerter such that both the available energy for harvesting at the EM and the secondary mass of the DVA benefitted from inertance magnification.

In this work, the dual performance of the EH-TMDI configuration for energy harvesting and vibration suppression is assessed, for the first time in the literature, for random white noise excited SDOF as well as MDOF structures as the inertance increases. In this respect, this study extends significantly the work by Salvi and Giaralis (2016) by considering frequency domain random vibration analyses of EH-TMDI equipped SDOF primary structures to gauge the performance of the EH-TMDI under broadband excitations instead of a single-harmonic deterministically defined load. This is an important consideration as performance of regenerative DVAs under random broadband excitation may significantly differ from harmonic excitations (e.g., Adhikari et al. 2009, Shen et al. 2019). Moreover, the herein paper generalizes the EH-TMDI configuration to treat lumped-mass MDOF primary structures in which the inerter is not grounded. For the latter class of systems, attention is focused on studying the influence stiffness properties of the primary to the EH-TMDI performance, which is known to critically affect the performance of non-regenerative TMDI (Wang and Giaralis 2021), under sets of external random white noise forces with different levels of correlation.

The remainder of the paper is organized as follows. Section 2 reviews the EH-TMDI configuration for SDOF primary structures along and the associated equations of motion are derived in time domain and in frequency domain. Section 3 reports on a parametric study for assessing the energy harvesting potential and vibration suppression performance of EH-TMDI for SDOF white noise excited structures. The study is underpinned by closed-form frequency domain random vibration analysis

Giaralis A. An inerter-based dynamic vibration absorber with concurrently enhanced energy harvesting and motion control performances under broadband stochastic excitation via inertance amplification. *ASCE-ASME Journal of Risk and Uncertainty in Engineering Systems Part B: Mechanical Engineering, accepted*: 16/11/2020.

solution to expedite the numerical calculation of statistics (variances) measuring the available energy for harvesting and the primary structure displacement. Section 4 defines the EH-TMDI configuration with non-grounded inerter for application to MDOF primary structures and derives its equations of motion. Numerical results from a parametric study assessing the performance of the novel EH-TMDI configuration with non-grounded inerter are reported facilitated by frequency domain closed-form random vibration analysis for correlated external random excitation. Finally, Section 5 summarizes main conclusions and provides future directions for further research.

2. Energy harvesting enabled tuned mass damper inerter (EH-TMDI) with grounded inerter

2.1 System modelling and definition of mechanical properties

Consider the class of dynamically excited structural systems amenable to be modelled as linear damped single degree of freedom (SDOF) oscillators with natural frequency, ω_s, and damping ratio, ζ_s, defined as

$$\omega_s = \sqrt{\frac{k_s}{m_s}} \quad , \quad \zeta_s = \frac{c_s}{2\sqrt{k_s m_s}} \tag{1}$$

In the above expressions, m_s is the mass, k_s is the stiffness, and c_s is the damping coefficient of the SDOF system. The oscillatory motion of such a system (primary structure) can be efficiently suppressed by the tuned mass-damper-inerter (TMDI) (Marian and Giaralis 2014): a passive linear vibration absorber coupling the classical linear TMD with a grounded inerter element as shown in Fig.1(a). Specifically, the TMDI comprises a (secondary) mass, m_T, which is attached to the primary structure via a linear spring with stiffness k_T in parallel with viscous damper with damping coefficient c_T and further connected to the ground via an inerter element with inertance b. By definition, the inerter element develops a resisting force given as (Smith 2002)

$$F_b(t) = b\left(\ddot{x}_2(t) - \ddot{x}_1(t)\right), \tag{2}$$

where x_1 and x_2 are the element end-displacements (see inlet of Fig.1(a)) and, hereafter, a dot over a symbol denotes differentiation with respect to time t. In this respect, a grounded inerter exerts a force equal to $b\ddot{x}_T$ to the secondary mass of a vibrating TMDI-equipped SDOF system supported on stationary ground, where x_T is the secondary mass displacement (see Fig.1(a)). Therefore, the TMDI with grounded inerter in Fig.1(a) is equivalent to a TMD with secondary mass equal to m_T+b (Marian and Giaralis 2017). This consideration motivates the following definitions for the TMDI natural frequency ω_T and damping ratio ζ_T

$$\omega_T = \sqrt{\frac{k_T}{m_T + b}} \quad , \quad \zeta_T = \frac{c_T}{2\sqrt{k_T\left(m_T + b\right)}} \tag{3}$$

Giaralis A. An inerter-based dynamic vibration absorber with concurrently enhanced energy harvesting and motion control performances under broadband stochastic excitation via inertance amplification. *ASCE-ASME Journal of Risk and Uncertainty in Engineering Systems Part B: Mechanical Engineering, accepted*: 16/11/2020.

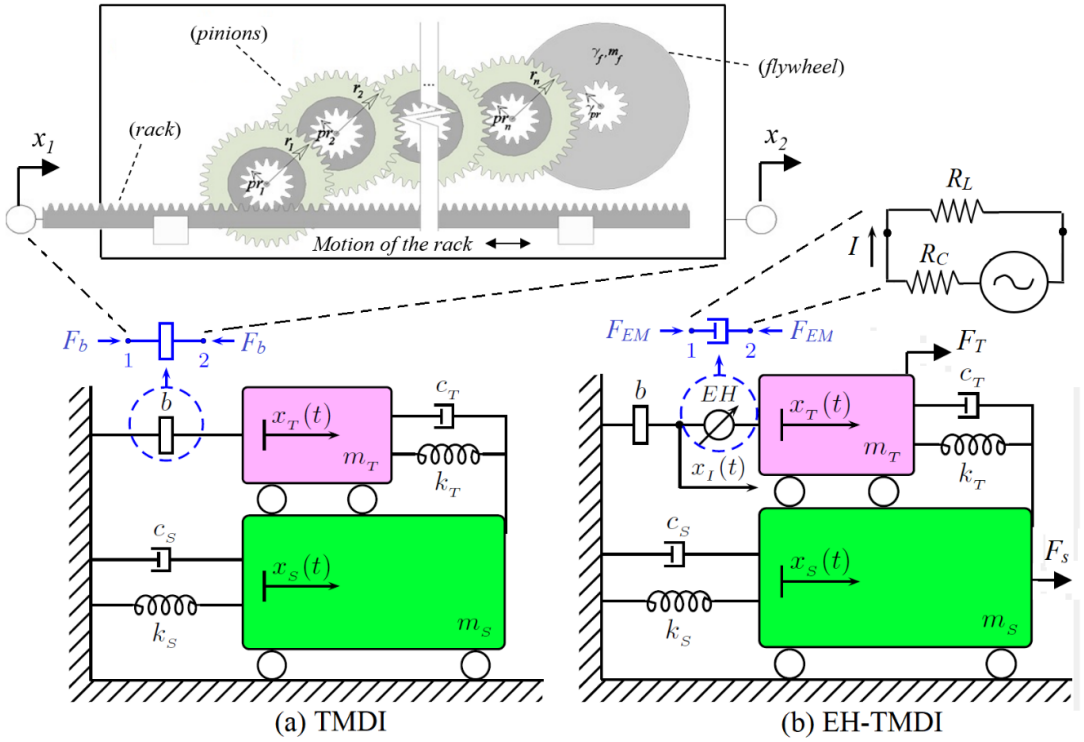

Figure 1. Mechanical models of damped SDOF primary structures equipped with (a) a tuned mass damper inerter (TMDI) with grounded rack-and-pinion flywheel-based inerter, and (b) an energy harvesting enabled tuned mass damper inerter (EH-TMDI) with grounded inerter and electromagnetic device coupled with a purely resistive electric load.

In this setting, the TMDI benefits significantly by the mass amplification effect of the grounded inerter compared to the conventional TMD (Marian and Giaralis 2014, 2017). This can be appreciated by noting that TMD vibration suppression efficacy improves monotonically as the secondary mass increases (e.g., De Angelis et al. 2012) and, at the same time, that the inertance is readily scalable in actual inerter device implementations (Smith 2020). The latter is commonly achieved by leveraging the rotational inertia of a flywheel driven by mechanisms which transform the relative translational motion of the device ends into rotational motion (e.g., Papageorgiou and Smith 2005, Pietrosanti et al. 2020). Elaborating further on the above concept, consider the idealized schematic in the inlet of Fig. 1(a) of a typical inerter device implementation incorporating a rack-and-pinion mechanism for linear-to-rotational motion transformation in tandem with gearing for rotational motion amplification of the flywheel. The inertance of such a device can be shown to be (Smith 2002)

$$b = m_f \frac{\gamma_f^2}{\gamma_{pr}^2}\left(\prod_{k=1}^{n}\frac{r_k^2}{pr_k^2}\right), \tag{4}$$

where m_f and γ_f are the mass and radius of the gyration of the flywheel, respectively, γ_{pf} is the radius of gyration of the flywheel pinion, $r_k/(pr_k)$ is the gearing ratio of the k-th stage/gear of the gearbox with n stages. It can be clearly deduced from Eq.(4) that the inertance can magnify by orders of magnitude with negligible change to the mass/weight of the device by increasing the mass and/or the inertia

Giaralis A. An inerter-based dynamic vibration absorber with concurrently enhanced energy harvesting and motion control performances under broadband stochastic excitation via inertance amplification. *ASCE-ASME Journal of Risk and Uncertainty in Engineering Systems Part B: Mechanical Engineering, accepted*: 16/11/2020.

properties of the flywheel (e.g., Hu et al. 2016, Pietrosanti et al. 2020) and/or the gearing ratio (e.g., Brzeski et al. 2017, Lazarek et al. 2019).

Building on the TMDI with varying inertance (Marian and Giaralis 2017, Pietrosanti et al. 2020), herein the energy harvesting-enabled tuned mass-damper-inerter (EH-TMDI) configuration shown in Fig.1(b) is put forth for simultaneous vibration suppression and dynamic energy harvesting from SDOF primary structures subject to random excitation. This configuration has been introduced by Salvi and Giaralis (2016) but its performance was studied only for harmonic excitations and for SDOF primary structures. In this work, the EH-TMDI configuration performance is studied for random broadband excitation and for SDOF as well as MDOF primary structures, not considered in the literature before.

The EH-TMDI incorporates a standard linear electromagnetic motor (EM), widely considered in the literature for extracting energy from large-amplitude low-frequency structural oscillations (e.g., Zhu et al. 2012, Zuo and Tang 2013, Gonzalez-Buelga et al. 2014), connected in series with the grounded inerter and the secondary mass. The EM consists of a magnet moving inside a coil with magnetic flux density B and electrical resistance R_c, while the inductance is taken as negligible which is a reasonable assumption for the considered application (e.g., Tang and Zuo 2012, Gonzalez-Buelga et al. 2014). The two ends of the EM coil are connected with a purely resistive circuit (load) with resistance R_L in which electric current I flows as seen in Fig.1(b). Whilst this simplified circuit modelling (shunt damping) does not account for potential nonlinear behaviour of actual energy harvesting circuits (e.g., Zhu et al. 2012), it is deemed sufficient for the comparative quantification of the available energy for harvesting pursued in this work (see also Marian and Giaralis 2017, Shen et al. 2019, Petrini et al. 2020) as the inertance of EH-TMDI is let to vary. Under the above assumptions, the EM develops a velocity-dependent resisting force (e.g., Palomera et al. 2008, Gonzalez-Buelga et al. 2014) equal to

$$F_{EM}\left(t\right)=c_{EM}\left(\dot{x}_2\left(t\right)-\dot{x}_1\left(t\right)\right), \tag{5}$$

in the mechanical domain, where

$$c_{EM}=\frac{\left(Bl\right)^2}{\left(R_C+R_L\right)}, \tag{6}$$

and l is the length of the EM moving magnet. In view of Eq.(5), it can be argued that the EM acts as a viscous damper with damping coefficient c_{EM}. To this end, an effective EM damping ratio is defined as

$$\zeta_{EM}=\frac{c_{EM}}{2\sqrt{k_T\left(m_T+b\right)}}=\zeta_p+\zeta_{EH}, \tag{7}$$

in analogy to the definition in Eq. (3). The above EM damping ratio, ζ_{EM}, ratio is taken equal to the sum of the damping ratio, ζ_p, associated with energy loss to heat (parasitic damping) and the damping ratio, ζ_{EH}, associated with the available energy for harvesting, that is, the energy dissipated at the resistive load R_L. (e.g., Gonzalez-Buelga et al. 2014).

Giaralis A. An inerter-based dynamic vibration absorber with concurrently enhanced energy harvesting and motion control performances under broadband stochastic excitation via inertance amplification. *ASCE-ASME Journal of Risk and Uncertainty in Engineering Systems Part B: Mechanical Engineering, accepted*: 16/11/2020.

2.2 Equations of motion and solution in frequency domain

The dynamic response of a EH-TMDI-equipped SDOF structural system can be expressed in terms of the three independent displacements (DOFs) indicated in Fig. 1(b). These are the displacement of the primary structure, x_s, the displacement of the secondary mass, x_T, and the displacement of the non-grounded inerter end, x_I. Herein, all three displacements are taken as being relative to the ground displacement. The equations of motion of this 3-DOF dynamical system exposed to the external dynamic forces F_s and F_T acting onto the primary structure and the secondary mass, respectively, are written as

$$\begin{cases} m_s\ddot{x}_s(t)+c_s\dot{x}_s(t)+c_T\left(\dot{x}_s(t)-\dot{x}_T(t)\right)+k_s x_s(t)+k_T\left(x_s(t)-x_T(t)\right)=F_s(t) \\ m_T\ddot{x}_T(t)+c_T\left(\dot{x}_T(t)-\dot{x}_s(t)\right)+k_T\left(x_T(t)-x_s(t)\right)+c_{EM}\left(\dot{x}_T(t)-\dot{x}_I(t)\right)=F_T(t) \\ c_{EM}\left(\dot{x}_I(t)-\dot{x}_T(t)\right)+b\ddot{x}_I(t)=0 \end{cases} \tag{8}$$

For the case of force-excited primary structures it is taken that $F_T=0$, while for the case of base-excited primary structures forces become $F_s=-m_s\ddot{x}_g(t)$ and $F_T=-m_T\ddot{x}_g(t)$ in Eq.(8) where $\ddot{x}_g(t)$ is the ground acceleration.

Dividing Eq.(8) by m_s and introducing the dimensionless mass ratio, μ, frequency ratio, f, and inertance ratio, β, defined as

$$\mu=\frac{m_T}{m_s} \quad , \quad f=\frac{\omega_T}{\omega_s}, \quad \text{and} \quad \beta=\frac{b}{m_s} \tag{9}$$

respectively, the system of equations in Eq.(8) can be written in matrix form as

$$\mathbf{M}\ddot{\mathbf{x}}(t)+\mathbf{C}\dot{\mathbf{x}}(t)+\mathbf{K}\mathbf{x}(t)=\mathbf{F}(t), \tag{10}$$

where

$$\mathbf{M}=\begin{bmatrix} 1 & 0 & 0 \\ 0 & \mu & 0 \\ 0 & 0 & \beta \end{bmatrix}$$

$$\mathbf{C}=\begin{bmatrix} 2\zeta_s\omega_s+2\zeta_T\omega_T(\mu+\beta) & -2\zeta_T\omega_T(\mu+\beta) & 0 \\ -2\zeta_T\omega_T(\mu+\beta) & 2(\zeta_T+\zeta_{EM})\omega_T(\mu+\beta) & -2\zeta_{EM}\omega_T(\mu+\beta) \\ 0 & -2\zeta_{EM}\omega_T(\mu+\beta) & 2\zeta_{EM}\omega_T(\mu+\beta) \end{bmatrix} \tag{11}$$

$$\mathbf{K}=\begin{bmatrix} \omega_s^2+\omega_T^2(\mu_T+\beta) & -\omega_T^2(\mu_T+\beta) & 0 \\ -\omega_T^2(\mu_T+\beta) & \omega_T^2(\mu_T+\beta) & 0 \\ 0 & 0 & 0 \end{bmatrix}$$

Giaralis A. An inerter-based dynamic vibration absorber with concurrently enhanced energy harvesting and motion control performances under broadband stochastic excitation via inertance amplification. *ASCE-ASME Journal of Risk and Uncertainty in Engineering Systems Part B: Mechanical Engineering, accepted*: 16/11/2020.

are the mass, damping, and stiffness matrices, respectively. Further, in Eq.(10) $\mathbf{x}(t)=\begin{bmatrix} x_s & x_T & x_I \end{bmatrix}^T$ is the displacement vector and $\mathbf{F}(t)=\begin{bmatrix} F_s/m_s & F_T/m_s & 0 \end{bmatrix}^T$ is the force vector, where the superscript "*T*" denotes matrix/vector transposition.

The equations of motion of the EH-TMDI-equipped SDOF structural system can be efficiently solved in the frequency domain by dividing Eq.(10) by ω_s^2, applying the Fourier transform and solving for the vector $\hat{\mathbf{X}}(g)=\begin{bmatrix} \hat{X}_s(g) & \hat{X}_T(g) & \hat{X}_I(g) \end{bmatrix}^T$ which collects the Fourier transformed elements of the displacement vector $\mathbf{x}(t)$ written in terms of the normalised frequency $g=\omega/\omega_s$. The above operations yield

$$\hat{\mathbf{X}}(g)=\mathbf{H}(g)\hat{\mathbf{F}}(g), \tag{12}$$

where $\hat{\mathbf{F}}(g)=\begin{bmatrix} \hat{F}_s(g)/k_s & \hat{F}_T(g)/k_s & 0 \end{bmatrix}^T$ is the excitation vector collecting the Fourier transformed elements of the force vector $\mathbf{F}(t)$, and $\mathbf{H}(g)$ is the admittance matrix given as

$$\mathbf{H}(g)=\left(-g^2\mathbf{M}+ig\mathbf{C}+\mathbf{K}\right)^{-1}, \tag{13}$$

where $i=\sqrt{-1}$ and the superscript "-1" denotes matrix inversion. The elements of the admittance matrix in Eq.(13) are provided in the Appendix A.

2.3 Frequency response functions for different inertance values

The closed-form frequency domain solution in Eq.(12) is herein leveraged to gain insight on the influence of the inertance to the vibration suppression and energy harvesting potential of the EH-TMDI configuration in Fig.1(b). To this aim, the following normalised (dimensionless) frequency response functions (FRFs) are considered

$$N_s(g)=\left|\frac{\hat{X}_s(g)}{F_o/k_s}\right|,\quad N_T(g)=\left|\frac{\hat{X}_T(g)}{F_o/k_s}\right|,\quad \text{and}\quad P_{EH}(g)=\zeta_{EH}\,f\left(\mu+\beta\right)g^2\left|\frac{\hat{X}_T(g)-\hat{X}_I(g)}{F_o/k_s}\right|^2, \tag{14}$$

which are defined with the aid of the $\hat{\mathbf{X}}(g)$ displacement response vector in Eq.(12) for an EH-TMDI equipped SDOF system harmonically force-excited with amplitude F_o. Notably, the FRFs N_s and N_T in Eq.(14) trace the steady-state peak response displacement (dynamic amplification factor) of the primary structure and of the secondary mass, respectively, in the frequency domain. Further, the FRF P_{EH} can be viewed as a measure of the available energy for harvesting in the frequency domain (see also Gonzalez-Buelga et al. 2014, and Marian and Giaralis 2017). In this regard, the relevance of the inertance property in regulating the motion control and energy harvesting attributes of the EH-TMDI can be effectively investigated by juxtaposing plots of the FRFs in Eq.(14) for different inertance values. To facilitate a meaningful comparison, the stiffness, k_T, and damping coefficient, c_T, of the EH-TMDI or, equivalently, the frequency ratio f in Eq. (9) and damping ratio ζ_T in Eq.(3) need to be tuned such

Giaralis A. An inerter-based dynamic vibration absorber with concurrently enhanced energy harvesting and motion control performances under broadband stochastic excitation via inertance amplification. *ASCE-ASME Journal of Risk and Uncertainty in Engineering Systems Part B: Mechanical Engineering, accepted*: 16/11/2020.

that inertance is accounted for. This consideration is herein fulfilled by using the tuning formulae (Marian and Giaralis 2017)

$$f = \frac{1}{1+\beta+\mu} \quad \text{and} \quad \zeta_T = \sqrt{\frac{3(\mu+\beta)}{8(1+\mu+\beta)}}\ , \tag{15}$$

which are functions of the inertance ratio β in Eq.(9). Note that the above formulae minimise the peak response of TMDI-equipped undamped SDOF oscillators (i.e., the system in Fig.1(a) with c_s=0) under harmonic force-excitation.

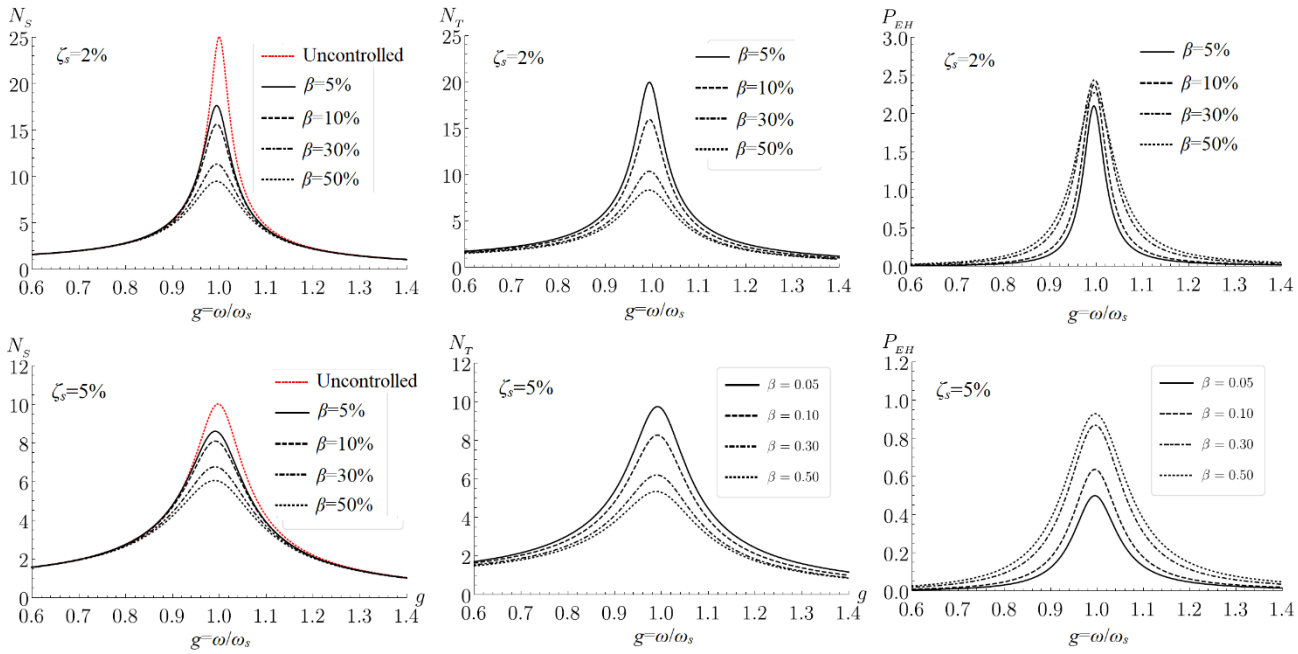

Figure 2. Dimensionless frequency response functions in Eq. (14) for various inertance ratios β, structural damping ratios ζ_s=2% and 5%, mass ratio μ=1%, parasitic damping ratio ζ_p=1%, and energy harvesting ratio ζ_{EH}=10%.

In this setting, Fig.2 plots FRFs in Eq.(14) for four different inertance ratio values, β=5%,10%, 30%, and 50%, and two different inherent damping ratio values, ζ_s= 2% and 5%. The mass ratio is taken fixed and equal to a relatively low value, μ=1%, motivated by the fact that TMDI in Fig.1(a) becomes more efficient for low secondary mass and large inertance (e.g., Marian and Giaralis 2014, De Angelis et al. 2019). Similarly, the parasitic and energy harvesting damping ratios are taken fixed and equal to ζ_p= 1% and ζ_{EH}= 10%, respectively, in line with experimental setups of typical regenerative TMDs (e.g., Zhu et al. 2012, Gonzalez-Buelga et al. 2014). It is seen that as the inertance increases (e.g., through gearing-up the rack-and-pinion inerter in Fig.1(a)) the EH-TMDI becomes more effective in suppressing the displacement amplitudes for both the primary structure and secondary mass while, simultaneously, increases the available energy for harvesting at the EM across all frequencies. It is further noted that the improvements in vibration suppression and energy harvesting saturate as the inertance increases and depend heavily on the inherent structural damping.

Giaralis A. An inerter-based dynamic vibration absorber with concurrently enhanced energy harvesting and motion control performances under broadband stochastic excitation via inertance amplification. *ASCE-ASME Journal of Risk and Uncertainty in Engineering Systems Part B: Mechanical Engineering, accepted*: 16/11/2020.

As a final remark, it is worth noting that the frequency range within which the increase of EH-TMDI inertance reduces the primary structure motion amplitude is much narrower (i.e., within a band of ±5% of the resonant excitation frequency g=1) compared to the frequency range that the available energy for harvesting increases. In fact, the latter range broadens significantly with the inherent primary structure damping. In this regard, the investigation of the concurrent motion control performance and energy generation potential of the EH-TMDI configuration to broadband/white random noise excitation for increasing inertance becomes relevant and is addressed in subsequent sections. In the interim, it is deemed important to highlight that the simultaneous improvement of both vibration suppression capability and energy harvesting potential for resonant excitation g=1 as the inertance is let to increase is a unique attribute of the EH-TMDI configuration in Fig. 1(b), not shared by alternative inerter-based DVAs with energy generation capabilities studied in the literature (e.g., Marian and Giaralis 2017, Luo et al. 2017, Joubaneh and Barry 2019, Zhu et al. 2019, Petrini et al. 2020). To highlight this fact, Fig. B1 in Appendix B compares the FRF plots in Fig.2 with corresponding FRF plots from two different DVA configurations considered in the literature for simultaneous vibration suppression and dynamics energy harvesting, while more detailed related discussion can be found in Salvi and Giaralis (2016).

3. Assessment of EH-TMDI with grounded inerter under white noise excitation

In this section, a novel parametric investigation is undertaken to assess the performance of the EH-TMDI configuration with grounded inerter in Fig.1(b) as inertance increases for vibration suppression and energy generation in SDOF systems subject to broadband/white random noise excitation. The cases of force-excited and base-excited structures are treated. To this aim, the following dimensionless performance indices (PIs) are adopted

$$I_S = \frac{\sigma_{\dot{x}_s}^2}{D} \quad \text{and} \quad I_{EH} = \zeta_{EH} f\left(\mu+\beta\right)\frac{\sigma_{\dot{x}_T-\dot{x}_I}^2}{D}. \tag{16}$$

In the above expressions, I_S is proportional to the variance of the primary structure deflection, $\sigma_{x_s}^2$, and is used to quantify the achieved level of vibration suppression by the EH-TMDI, while I_{EH} is proportional to the product of an effective damping coefficient corresponding to the energy harvested by the EM (see Eq.(7)) and the variance of the relative velocity at the ends of the EM, $\sigma_{\dot{x}_T-\dot{x}_I}^2$. The latter PI is widely used to gauge energy harvesting potential in randomly excited DVAs (e.g., Adhikari et al. 2009, Tang and Zuo 2012). Further, the denominator D ensures that the PIs are unitless and is given as

$$D = \frac{2\pi S_F \omega_s}{k_s^2} \quad or \quad D = \frac{2\pi S_A}{\omega_s^3}, \tag{17}$$

for force-excited and base-excited primary structure, respectively, where S_F is the spectral amplitude of the white noise force excitation process, while $S_A = S_F / m_s^2$ is the spectral amplitude of the white noise base acceleration excitation process.

The PIs in Eq. (16) can be expressed using the admittance matrix elements in Eq.(13) as

Giaralis A. An inerter-based dynamic vibration absorber with concurrently enhanced energy harvesting and motion control performances under broadband stochastic excitation via inertance amplification. *ASCE-ASME Journal of Risk and Uncertainty in Engineering Systems Part B: Mechanical Engineering, accepted*: 16/11/2020.

$$I_S = \int_{-\infty}^{\infty} H_s(g)\,dg \quad \text{and} \quad I_{EH} = \zeta_{EH} f(\mu+\beta) \int_{-\infty}^{\infty} g^2 \left[H_T(g) + H_I(g) - 2\sqrt{H_{TI}(g) H_{IT}(g)} \right] dg\,, \tag{18}$$

where

$$\begin{aligned} &H_s(g) = \left| \frac{H_{11}(g)}{\Delta} \right|^2, \quad H_T(g) = \left| \frac{H_{21}(g)}{\Delta} \right|^2, \quad H_I(g) = \left| \frac{H_{31}(g)}{\Delta} \right|^2, \\ &H_{TI}(g) = \frac{H_{21}(g) H_{31}^*(g)}{|\Delta|^2}, \quad H_{IT}(g) = \frac{H_{31}(g) H_{21}^*(g)}{|\Delta|^2} \end{aligned} \tag{19}$$

for force-excited primary structures and

$$\begin{aligned} &H_s(g) = \left| \frac{H_{11}(g)}{\Delta} \right|^2 + \mu \left| \frac{H_{12}(g)}{\Delta} \right|^2, \quad H_T(g) = \left| \frac{H_{21}(g)}{\Delta} \right|^2 + \mu \left| \frac{H_{22}(g)}{\Delta} \right|^2, \\ &H_I(g) = \left| \frac{H_{31}(g)}{\Delta} \right|^2 + \mu \left| \frac{H_{32}(g)}{\Delta} \right|^2, \\ &H_{TI}(g) = \frac{H_{21}(g) H_{31}^*(g)}{|\Delta|^2} + \mu \frac{H_{22}(g) H_{32}^*(g)}{|\Delta|^2}, \quad H_{IT}(g) = \frac{H_{31}(g) H_{21}^*(g)}{|\Delta|^2} + \mu \frac{H_{32}(g) H_{22}^*(g)}{|\Delta|^2} \end{aligned} \tag{20}$$

for base-excited primary structures. In the last two equations, $\Delta = \det(-g^2\mathbf{M} + ig\mathbf{C} + \mathbf{K})$ and the superscript "*" denotes complex conjugation.

To ensure a meaningful comparison of PIs in Eq.(18) as inertance scales-up, it is deemed essential to tune the frequency ratio f in Eq. (9) and the damping ratio ζ_T in Eq.(3) to account the varying inerter ratio β as previously discussed. To this end, the following tuning formulae

$$f = \frac{1}{1+\beta+\mu} \sqrt{\frac{2+\mu+\beta}{2}} \quad \text{and} \quad \zeta_T = \sqrt{\frac{(\mu+\beta)\left[4+3(\mu+\beta)\right]}{8(1+\mu+\beta)(2+\mu+\beta)}}, \tag{21}$$

are adopted for force-excited primary structures, and the following tuning formulae

$$f = \frac{1}{1+\beta+\mu} \sqrt{\frac{2-\mu-\beta}{2}} \quad \text{and} \quad \zeta_T = \sqrt{\frac{(\mu+\beta)(4-\mu-\beta)}{8(1+\mu+\beta)(2-\mu-\beta)}}, \tag{22}$$

are adopted for base-excited primary structures. The expressions in Eq.(21) and Eq.(22) provide optimal tuning parameters for the classical TMD (i.e., DVA configuration in Fig.1(a) with no inerter) with mass ratio $\mu+\beta$ for undamped SDOF primary structures under white noise force excitation and white noise base acceleration excitation, respectively, derived by Warburton (1982). The rationale behind this tuning strategy relates to the fact that a TMDI with grounded inerter and with inertance ratio β and mass ratio μ behaves as a TMD with mass ratio $\mu+\beta$ for force-excited SDOF primary structure (see section

Giaralis A. An inerter-based dynamic vibration absorber with concurrently enhanced energy harvesting and motion control performances under broadband stochastic excitation via inertance amplification. *ASCE-ASME Journal of Risk and Uncertainty in Engineering Systems Part B: Mechanical Engineering, accepted*: 16/11/2020.

2.1). In this respect, whilst it is recognized that the tuning formulae in Eqs.(21) and (22) do not optimize the performance of the EH-TMDI against any particular criterion, they do serve well the purpose of supporting a fair parametric comparative study of the EH-TMDI motion control and energy harvesting attributes.

In this context, Fig. 3 plots the PIs defined in Eq.(16) as functions of the inertance ratio β for white noise force-excited primary structures using equations Eqs.(18), (19), and (21) in conjunction with standard quadrature implemented in MATLAB® for the numerical evaluation of the integrals in Eq.(18). In each panel of Fig.3, EH-TMDI equipped SDOF primary structures with different system properties are considered as indicated on the Figure while the parasitic damping ratio is taken equal to 1% for all systems. The PIs are normalized to the peak value attained in each panel to facilitate a comparison between them as the inertance scales up.

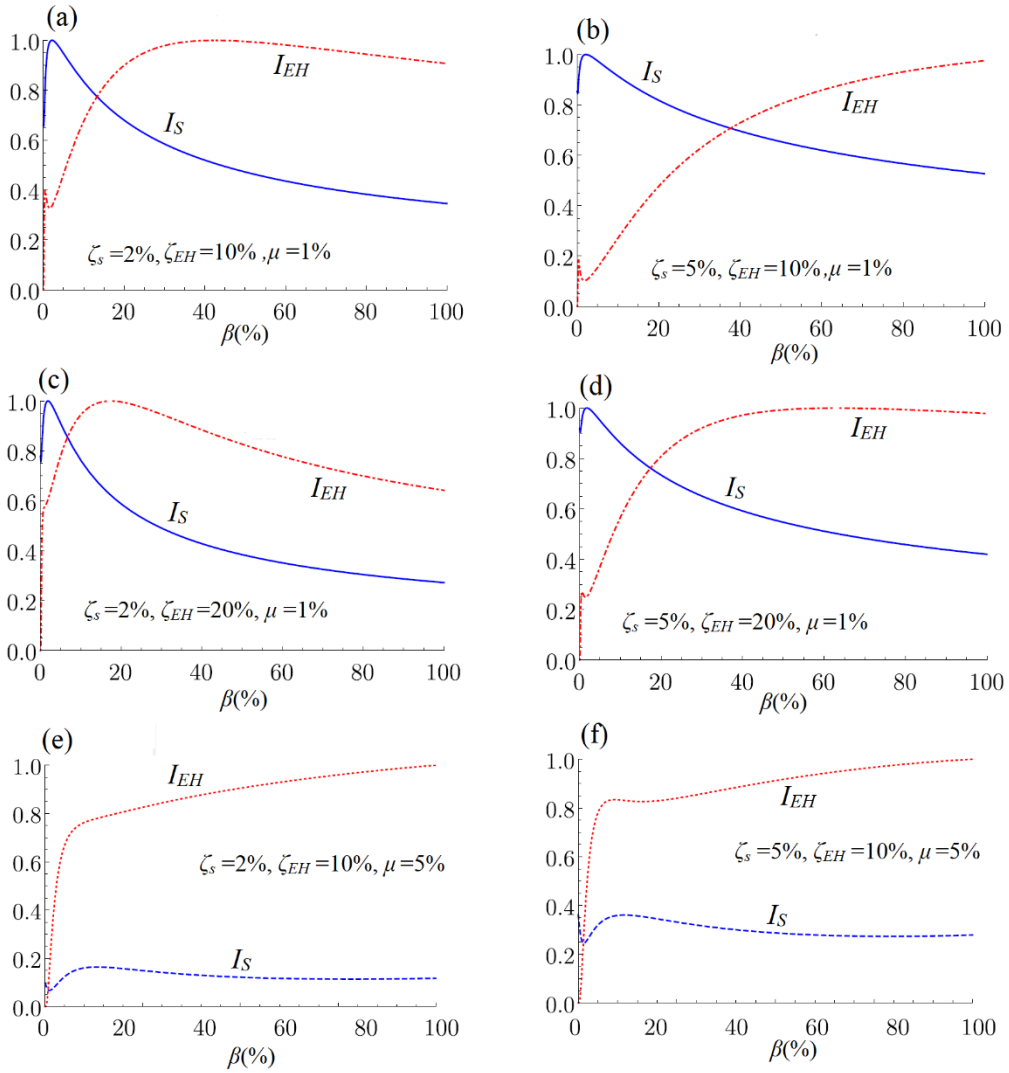

Figure 3. Motion control and energy harvesting performance indices in Eq. (16) normalized to their peak value for different white noise force-excited EH-TMDI-equipped SDOF primary structures with ζ_p=1%.

Giaralis A. An inerter-based dynamic vibration absorber with concurrently enhanced energy harvesting and motion control performances under broadband stochastic excitation via inertance amplification. *ASCE-ASME Journal of Risk and Uncertainty in Engineering Systems Part B: Mechanical Engineering, accepted*: 16/11/2020.

Focusing first on the case of relatively lightweight EH-TMDIs with secondary mass μ=1% (Figs. 3(a)-(d)), it is seen that their capability to control the primary structure displacement improves monotonically with the inertance ratio for β>3% as evidenced by the constantly decreasing I_S index trends with increasing inertance. This improving trend (i.e., monotonic decrease of I_S curves with inertance) holds irrespective of the inherent structural damping ratio, ζ_s, and the damping effect due to energy harvesting as expressed through the damping ratio ζ_s. However, the rate of improvement of the EH-TMDI motion control capability saturates as the inertance ratio increase. Interestingly, this is also the case for the motion control capability of the TMDI in Fig.1(a) as reported in the literature (see e.g., Marian and Giaralis 2014, De Angelis et al. 2019) and, in this regard, inertance scaling-up affects the motion control capability of the EH-TMDI and TMDI in a similar manner. More importantly, the EH-TMDI available energy for harvesting increases as well with the inertance as manifested by the I_{EH} index increasing trends in Figs. 3(a)-(d). However, I_{EH} increasing trend with inertance is monotonic only for the primary structure with the relatively large inherent damping, ζ_s=5%, typical of reinforced concrete structures (Figs.3(b) and (d)). Indeed, for the lighter damped primary structure with ζ_s=2% (commonly assumed for steel structures) in Figs.3(a) and (c), the I_{EH} curve reduces after attaining a local maximum. This observation suggests that for relatively lightly damped primary structures and lightweight EH-TMDIs there is a critical inertance value above which the increase of inertance becomes detrimental to the energy harvesting potential (though not to the vibration suppression capability of the EH-TMDI). In this respect, it is further worth noting that by increasing the energy harvesting damping ratio, ζ_{EH}, all the I_{EH}-β plots shift to the left which, in turn, relaxes requirements of large inertance for enhanced energy generation. For example, the critical inertance ratio value which maximizes the I_{EH} index for the primary structure with ζ_s=2% reduces by 50% (i.e., from β=35% to β=17.5%) as the energy harvesting damping ratio doubles from ζ_{EH}=10% to ζ_{EH}=20% in Figs.3(a) and (c).

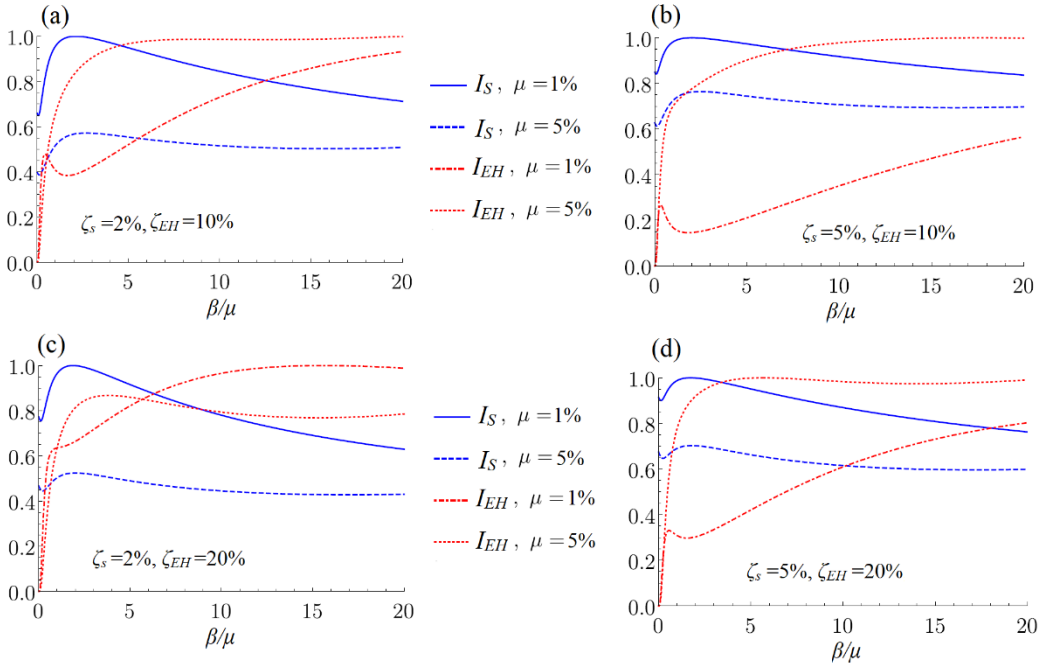

Figure 4. Motion control and energy harvesting performance indices in Eq. (16) normalized to their peak value for different white noise base acceleration excited EH-TMDI-equipped SDOF primary structures with ζ_p=1%.

Giaralis A. An inerter-based dynamic vibration absorber with concurrently enhanced energy harvesting and motion control performances under broadband stochastic excitation via inertance amplification. *ASCE-ASME Journal of Risk and Uncertainty in Engineering Systems Part B: Mechanical Engineering, accepted*: 16/11/2020.

Turning, next, the attention to the relatively heavyweight EH-TMDIs with μ=5% in Figs 3(e) and 3(f), it is seen that the energy harvesting potential of the EH-TMDI improves monotonically with inertance irrespective of the primary structure inherent damping. Still, the I_{EH}-β plots exhibit a distinct "bilinear" trend with a relatively low critical corner inertance value (~8%) above which the rate of improvement of I_{EH} with inertance (slope of the I_{EH}-β curves) drops dramatically. At the same time, the motion control capacity of the EH-TMDI is relatively insensitive to the inertance (i.e., I_S curves are almost flat). The latter observation confirms trends previously reported in the literature for the TMDI: the presence of an inerter benefits mostly lightweight TMD(I)s (see e.g., Marian and Giaralis 2014, De Angelis et al. 2019). To this end, it is evident that EH-TMDIs with large secondary mass do not benefit much from inertance scaling-up beyond a relatively low critical/corner inertance value for the dual purpose of energy harvesting and vibration suppression.

Further to the previously discussed numerical data, Fig.4 plots the PIs in Eq.(16) for white noise base acceleration excited SDOF primary structures using equations Eqs.(18), (20), and (22). Given that for base-excited systems both the primary structure and the secondary mass attract mass-proportional external forces, it is deemed useful for the sake of comparison to include on the same graph PIs from systems with different mass ratios μ. This is enabled by plotting the PIs in Fig.4 against the non-dimensional $\beta/\mu=b/m_T$ ratio. As in Fig.3, the system properties are indicated on the graphs, parasitic damping ratio is taken equal to 1% for all systems considered and PIs are normalized to the peak value attained in each panel of Fig.4. Collectively, all the trends of I_S and I_{EH} with inertance observed for the force-excited primary structures in Fig.3 are maintained for the base-excited structures in Fig.4 for all considered systems. In short, an increase to the secondary mass reduces the beneficial effect of the inertance in terms of vibration suppression, the latter being more substantial for lighter-damped primary structures. Further, better vibration suppression is achieved by increasing the energy harvesting damping ratio. In terms of energy harvesting potential, arguably, the most important observation to be made is the fact that the energy harvesting damping ratio has a most dramatic positive relative effect to the rate of energy harvesting improvement with inertance when a lightweight EH-TMDI is combined with a lightly damped primary structure (Fig.4(c)). Indeed, in this case, the available energy for harvesting for the EH-TMDI with μ=1% is higher compared to the EH-TMDI with μ=5% for all inertance values considered (note that due to the normalization of the x-axis inertance for $\mu=1\%$ is 5 times higher than inertance for μ=5% for fixed β/μ ratio). In view of the above, it is safe to conclude that even in the case of base-excited EH-TMDI equipped systems in which mass-proportional external kinetic energy enters the system through the secondary mass, having lightweight EH-TMDI with relatively large inertance is still more beneficial than heavyweight EH-TMDI in terms of both vibration suppression and energy harvesting.

4. Non-grounded EH-TMDI for multi-degree-of-freedom (MDOF) primary structures

4.1 System description and equations of motion

The thus far established beneficial effect of increasing inertance to the vibration suppression and energy harvesting potential of the EH-TMDI assumed the accessibility of a stationary acceleration reference (ground) to connect one end of the inerter as seen in Fig.1(b). In this setting, the inerter is engaged by the relative system kinematics with respect to the ground which is relevant even for base-excited systems since motion suppression and energy harvesting look at the relative to the ground kinematics. Nevertheless, the practical applicability of EH-TMDI with grounded inerter is limited to primary

Giaralis A. An inerter-based dynamic vibration absorber with concurrently enhanced energy harvesting and motion control performances under broadband stochastic excitation via inertance amplification. *ASCE-ASME Journal of Risk and Uncertainty in Engineering Systems Part B: Mechanical Engineering, accepted*: 16/11/2020.

structures in which the location of critical/maximum deflections are close to their supports/ground such as in seismically isolated structures and components (see e.g., De Angelis et al. 2019). However, peak deflections in most of typical slender structures and structural components develop naturally away from their supports (e.g., cantilevered or simply supported primary structures). In this regard, an innovative EH-TMDI configuration is herein proposed in which the inerter is not grounded but rather connects the EM to the primary structure at a location that is different from where the secondary mass is attached to via the parallel spring/damper connection. This is in analogy to several works on the TMDI with non-grounded inerter for vibration suppression of cantilevered structures including buildings (e.g., Marian and Giaralis 2013, Giaralis and Petrini 2017, Giaralis and Taflanidis 2018) and wind turbines (e.g., Sarkar and Fitzgerald 2020), as well as in multi-span bridge decks (e.g., Dai et al. 2019) commonly modelled as lumped-mass multi degree of freedom (MDOF) systems. To this end, a system with a force-excited 2-DOF linear damped primary structure is studied in this section with two lumped masses connected by an EH-TMDI as shown in Fig.5. In this configuration, the inerter is engaged by the relative dynamics of the two masses which, in turn, depend on the properties of the primary structure and the loading attributes (see also Wang and Giaralis 2021).

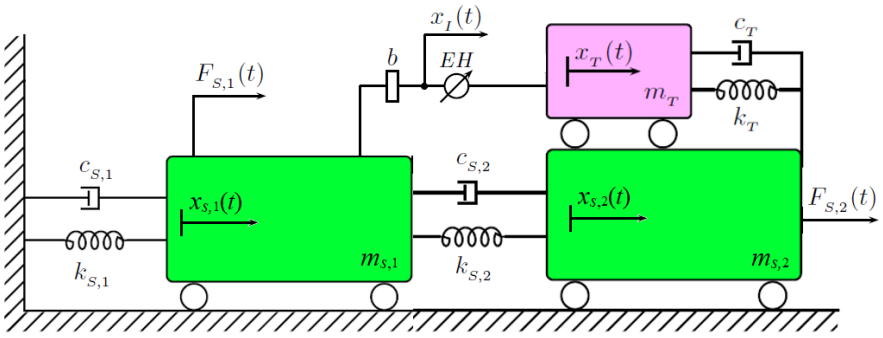

Figure 5. Mechanical model of a damped 2-DOF primary structure equipped with an EH-TMDI with non-grounded inerter.

Similar to the system in Fig.1(b), the dynamic response of the herein considered EH-TMDI-equipped 2-DOF structural system is written in terms of the four independent displacements indicated in Fig.5. These are the displacements of the two primary structure lumped masses, $x_{s,1}$ and $x_{s,2}$, the displacement of the secondary mass, x_T, and the displacement of the connection of the inerter with the EM, x_I. The equations of motion of this 4-DOF dynamical system exposed to the external dynamic forces $F_{s,1}$ and $F_{s,2}$ acting onto the primary structure masses as seen in Fig.4 are written as

$$\begin{cases} m_{s,1}\ddot{x}_{s,1}(t)+c_{s,1}\dot{x}_{s,1}(t)+c_{s,2}\left(\dot{x}_{s,1}(t)-\dot{x}_{s,2}(t)\right)+k_s x_{s,1}(t)+k_{s,2}\left(x_{s,1}(t)-x_{s,2}(t)\right)-b\left(\ddot{x}_I(t)-\ddot{x}_{s,1}(t)\right)=F_{s,1}(t) \\ m_{s,2}\ddot{x}_{s,2}(t)+c_{s,2}\left(\dot{x}_{s,2}(t)-\dot{x}_{s,1}(t)\right)+c_T\left(\dot{x}_{s,2}(t)-\dot{x}_T(t)\right)+k_{s,2}\left(x_{s,2}(t)-x_{s,1}(t)\right)+k_T\left(x_{s,2}(t)-x_T(t)\right)=F_{s,2}(t) \\ m_T\ddot{x}_T(t)+c_T\left(\dot{x}_T(t)-\dot{x}_{s,2}(t)\right)+k_T\left(x_T(t)-x_{s,2}(t)\right)+c_{EM}\left(\dot{x}_T(t)-\dot{x}_I(t)\right)=0 \\ b\left(\ddot{x}_I(t)-\ddot{x}_{s,1}(t)\right)-c_{EM}\left(\dot{x}_T(t)-\dot{x}_I(t)\right)=0 \end{cases} \quad (23)$$

The system of equations in Eq.(23) can be written in matrix form after dividing by $m_{s,1}$ as

$$\tilde{\mathbf{M}}\ddot{\tilde{\mathbf{x}}}(t)+\tilde{\mathbf{C}}\dot{\tilde{\mathbf{x}}}(t)+\tilde{\mathbf{K}}\tilde{\mathbf{x}}(t)=\tilde{\mathbf{F}}(t), \quad (24)$$

Giaralis A. An inerter-based dynamic vibration absorber with concurrently enhanced energy harvesting and motion control performances under broadband stochastic excitation via inertance amplification. *ASCE-ASME Journal of Risk and Uncertainty in Engineering Systems Part B: Mechanical Engineering, accepted*: 16/11/2020.

where $\tilde{\mathbf{x}}(t)=\begin{bmatrix} x_{s,1} & x_{s,2} & x_T & x_I \end{bmatrix}^T$ is the displacement vector, $\tilde{\mathbf{F}}(t)=\begin{bmatrix} F_{s,1}/m_{s,1} & F_{s,2}/m_{s,1} & 0 & 0 \end{bmatrix}^T$ is the force vector and the mass, damping, and stiffness matrices are given as

$$\tilde{\mathbf{M}}=\begin{bmatrix} 1+\beta & 0 & 0 & -\beta \\ 0 & \mu_s & 0 & 0 \\ 0 & 0 & \mu_T & 0 \\ -\beta & 0 & 0 & \beta \end{bmatrix}$$

$$\tilde{\mathbf{C}}=\begin{bmatrix} 2\zeta_{s,1}\omega_{s,1}+2\zeta_{s,2}\omega_{s,2}\mu_s & -2\zeta_{s,2}\omega_{s,2}\mu_s & 0 & 0 \\ -2\zeta_{s,2}\omega_{s,2}\mu_s & 2\zeta_{s,2}\omega_{s,2}\mu_s+2\zeta_T\omega_T(\mu_T+\beta) & -2\zeta_T\omega_T(\mu_T+\beta) & 0 \\ 0 & -2\zeta_T\omega_T(\mu_T+\beta) & 2(\zeta_T+\zeta_{EM})\omega_T(\mu_T+\beta) & -2\zeta_{EM}\omega_T(\mu_T+\beta) \\ -\beta & 0 & -2\zeta_{EM}\omega_T(\mu_T+\beta) & 2\zeta_{EM}\omega_T(\mu_T+\beta) \end{bmatrix} \quad (25)$$

$$\tilde{\mathbf{K}}=\begin{bmatrix} \omega_{s,1}^2+\omega_{s,2}^2\mu_s & -\omega_{s,2}^2\mu_s & 0 & 0 \\ -\omega_{s,2}^2\mu_s & \omega_{s,2}^2\mu_s+\omega_T^2(\mu_T+\beta) & -\omega_T^2(\mu_T+\beta) & 0 \\ 0 & -\omega_T^2(\mu_T+\beta) & \omega_T^2(\mu_T+\beta) & 0 \\ 0 & 0 & 0 & 0 \end{bmatrix}$$

respectively. In the above matrices the following non-modal dynamic properties (structural frequencies and damping ratios) of the primary structure have been used

$$\omega_{s,1}=\sqrt{\frac{k_{s,1}}{m_{s,1}}} \quad , \quad \omega_{s,2}=\sqrt{\frac{k_{s,2}}{m_{s,2}}} \quad , \quad \zeta_{s,1}=\frac{c_{s,1}}{2\sqrt{k_{s,1}m_{s,1}}}, \quad \text{and} \quad \zeta_{s,2}=\frac{c_{s,2}}{2\sqrt{k_{s,2}m_{s,2}}} \quad (26)$$

as well as the inertial (mass and inertance) ratios

$$\mu_s=\frac{m_{s,2}}{m_{s,1}} \quad , \quad \mu_T=\frac{m_T}{m_{s,1}}, \quad \text{and} \quad \beta=\frac{b}{m_{s,1}} \quad (27)$$

4.2 Parametric stochastic load modelling and frequency domain random vibrations analysis

The external dynamic loading applied to the considered 4-DOF system in Fig.5 is defined by a set of random white noise forces $F_{s,1}$ and $F_{s,2}$ exerted to the two lumped masses of the primary structure. The loading is herein represented by the power spectral density matrix

$$\mathbf{W}=\frac{S_o}{m_{s,1}^2}\begin{bmatrix} \alpha & \sqrt{\alpha}\rho & 0 & 0 \\ \sqrt{\alpha}\rho & 1 & 0 & 0 \\ 0 & 0 & 0 & 0 \\ 0 & 0 & 0 & 0 \end{bmatrix} \quad (28)$$

which supports an efficient random vibration analysis in frequency domain of the 4-DOF as detailed further below. In Eq.(28), S_o is the spectral amplitude of the $F_{s,2}$ white noise process, α is the ratio of

Giaralis A. An inerter-based dynamic vibration absorber with concurrently enhanced energy harvesting and motion control performances under broadband stochastic excitation via inertance amplification. *ASCE-ASME Journal of Risk and Uncertainty in Engineering Systems Part B: Mechanical Engineering, accepted*: 16/11/2020.

the spectral amplitudes of the $F_{s,1}$ over the $F_{s,2}$ white noise processes, and ρ is the correlation between $F_{s,1}$ and $F_{s,2}$ processes. In this regard, the provision of different α and ρ values enables a parametric investigation on the influence of the relative amplitude and correlation of the externally applied random forces to the primary structure, respectively. This includes the limiting cases of external force applied only to the lead mass of the primary structure (α=0) and of uncorrelated forces (ρ=0).

The response power spectral density matrix can be determined in closed-form by the standard input-output expression of random vibrations

$$\mathbf{S}(\tilde{g}) = \left(\mathbf{Z}(\tilde{g})\right)^{-1} \mathbf{W} \left(\mathbf{Z}^{*}(\tilde{g})\right)^{-1}, \tag{29}$$

where the superscript "*" denotes matrix conjugate transposition and **Z** is the impedance matrix defined as

$$\mathbf{Z}(\tilde{g}) = -\tilde{g}^2 \tilde{\mathbf{M}} + i\tilde{g}\tilde{\mathbf{C}} + \tilde{\mathbf{K}}, \tag{30}$$

in which $\tilde{g} = \omega / \omega_{s,1}$ is a normalized frequency. The elements of the impedance matrix are provided in the Appendix A.

4.3 Assessment of EH-TMDI with non-grounded inerter under white noise excitation

Herein, the performance of the EH-TMDI with non-grounded inerter in Fig.5 is assessed for concurrent motion control and energy generation as inertance scales up. For this purpose, the following two PIs are adopted

$$I_{x2} = \int_{-\infty}^{\infty} S_{22}(\tilde{g})\, d\tilde{g} \quad \text{and} \quad I_{EH2} = \zeta_{EH} f_T (\mu_T + \beta) \int_{-\infty}^{\infty} \tilde{g}^2 \left[S_{33}(\tilde{g}) + S_{44}(\tilde{g}) - 2\sqrt{S_{34}(\tilde{g}) S_{43}(\tilde{g})} \right] d\tilde{g}, \tag{31}$$

where S_{kj} is the [k,j] element of matrix **S** in Eq.(29) and $f_T = \omega_T/\omega_{s,1}$. The first PI in Eq.(31), I_{x2}, is the displacement variance of the lead mass of the 2-DOF primary structure which is used to gauge the vibration suppression achieved by the EH-TMDI. The second PI in Eq.(31), I_{EH2}, is the available energy for harvesting at the EM which is used to quantify the energy generation potential of the EH-TMDI.

In all cases considered, an inertance-dependent EH-TMDI tuning is adopted using the formulae in Eq.(21), applicable for white noise force-excited primary structure, with the understanding that this tuning does not yield optimal performance against any specific criterion. In the parametric investigation, attention is focused on the effects of the 2-DOF primary structure stiffness properties, expressed by the relative stiffness ratio

$$\gamma_s = \frac{k_{s,2}}{k_{s,1}}, \tag{32}$$

Giaralis A. An inerter-based dynamic vibration absorber with concurrently enhanced energy harvesting and motion control performances under broadband stochastic excitation via inertance amplification. *ASCE-ASME Journal of Risk and Uncertainty in Engineering Systems Part B: Mechanical Engineering, accepted*: 16/11/2020.

in conjunction with the attributes of the external random loading, namely the correlation and the spectral amplitude ratios ρ and a in Eq.(28). This is because the effects of the damping and secondary mass properties to the EH-TMDI performance have already been thoroughly examined in Section 3, while it has been recently shown that the primary structure stiffness affect significantly the vibration suppression performance of the TMDI in MDOF structures (Wang and Giaralis 2021). In this regard, for all structures considered, the inherent damping properties of the primary structure are taken fixed as $\zeta_{s,1}$= $\zeta_{s,1}$=5%, the energy harvesting ratio is also taken fixed as ζ_{EH}= 10%, the parasitic damping is ζ_p= 1% and the secondary mass ratio is μ_T= 1%.

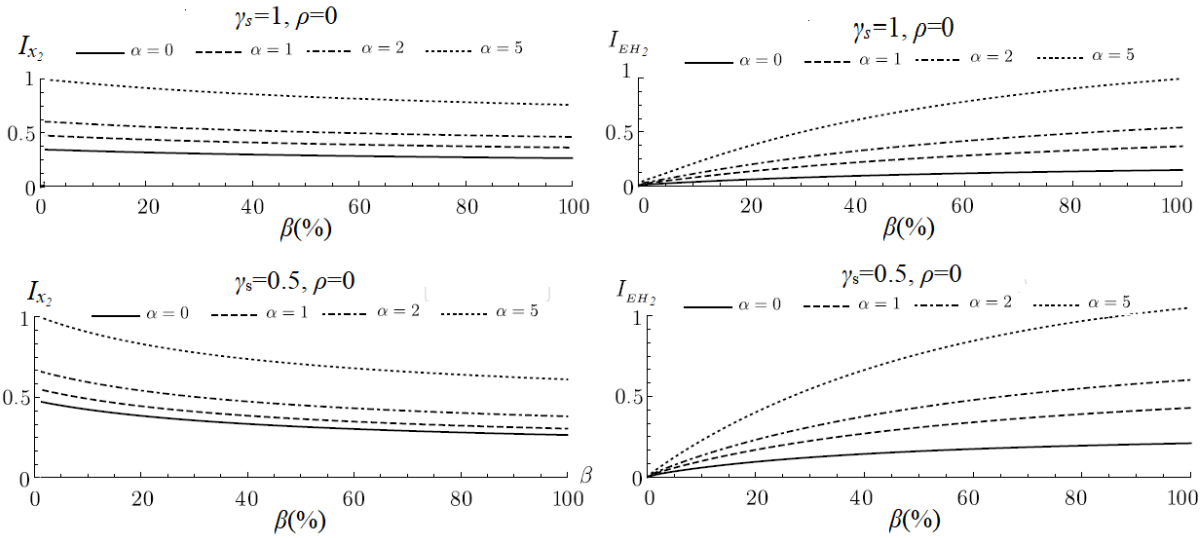

Figure 6. Motion control and energy harvesting performance indices in Eq. (33) normalized to their peak value for uncorrelated (ρ=0) white noise force-excited EH-TMDI-equipped 2-DOF primary structures with $\zeta_{s,1}$= $\zeta_{s,1}$=5%, ζ_{EH}= 10%, ζ_p=1%, μ_T= 1%, and μ_s=1, plotted against the inertance ratio β.

Figure 6 plots the PIs in Eq.(33) as functions of the inertance ratio β for uncorrelated external white noise forces (i.e., ρ=0 in Eq.(28)) with different spectral amplitude ratio values α, μ_s=1, and for two values of relative stiffness ratio γ_s=1 and γ_s=0.5, or, equivalently, f_s= $\omega_{s,2}/\omega_{s,1}$=1 and f_s= $\sqrt{1/2}$. As before, the PIs are normalized to the peak value attained in each panel for the sake of comparison. It is seen that for any given inertance value, the vibration suppression performance of EH-TMDI deteriorates (i.e., lead mass displacement variance I_{x2} increases), while the energy generation potential improves (i.e., available energy for harvesting I_{EH} increases) as the spectral ratio increases from α=0 (external force is exerted only to the lead mass $m_{s,2}$) to α=5. However, for any fixed spectral force ratio α, the EH-TMDI motion control and energy harvesting performances improve concurrently as the inertance scales up. These improvements are more significant as α increases and/or as the stiffness ratio γ_s reduces (i.e., as the spring connecting the two primary structure masses becomes more flexible compared to the spring supporting the primary structure to the ground).

To shed more light on the effect of the stiffness ratio to the EH-TMDI performance, Fig.7 plots the two PIs in Eq.(31) with inertance for μ_s=0.1 and for three different values of γ_s= 0.1, 0.5, and 1 or, equivalently, f_s= $\omega_{s,2}/\omega_{s,1}$=1, $\sqrt{5}$, and $\sqrt{10}$. It is clearly seen that as the stiffness ratio reduces, the rate of concurrent improvement of both the EH-TMDI vibration suppression and energy harvesting performances with inertance increases. Nevertheless, it is also seen that for any fixed inertance value,

Giaralis A. An inerter-based dynamic vibration absorber with concurrently enhanced energy harvesting and motion control performances under broadband stochastic excitation via inertance amplification. *ASCE-ASME Journal of Risk and Uncertainty in Engineering Systems Part B: Mechanical Engineering, accepted*: 16/11/2020.

the lead mass displacement increases as the stiffness ratio reduces while the opposite holds for the available energy for harvesting. Therefore, care needs to be exercised in increasing the flexibility of the connection of the two primary masses as this may lead to excessive lead mass displacement. Still, lead mass displacement can be efficiently rectified by scaling up the inertance which, remarkably, increases the available energy for harvesting.

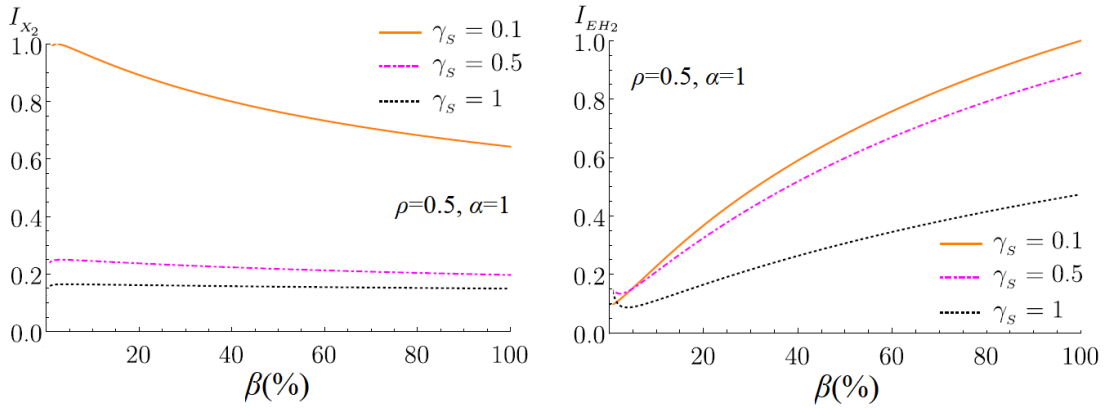

Figure 7. Motion control and energy harvesting performance indices in Eq. (33) normalized to their peak value for correlated (ρ=0.5) white noise force-excited EH-TMDI-equipped 2-DOF primary structures with various values of stiffness ratio γs, and with $\zeta_{s,1}$= $\zeta_{s,1}$=5%, ζ_{EH}= 10%, ζ_p=1%, μ_T= 1%, and μ_s=0.1, plotted against the inertance ratio β.

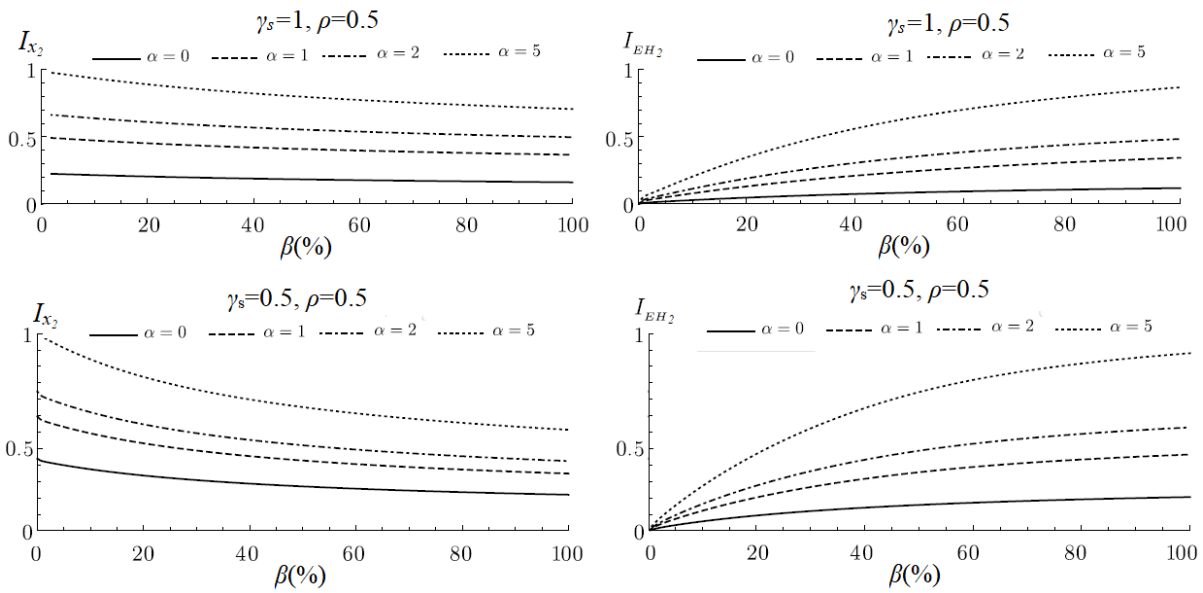

Figure 8. Motion control and energy harvesting performance indices in Eq. (33) normalized to their peak value for correlated (ρ=0.5) white noise force-excited EH-TMDI-equipped 2-DOF primary structures with $\zeta_{s,1}$= $\zeta_{s,1}$=5%, ζ_{EH}= 10%, ζ_p=1%, μ_T= 1%, and μ_s=1, plotted against the inertance ratio β.

Further to the above, Fig. 8 plots the same data as Fig.6 but for correlated external white forces with ρ=0.5. The trends of the PIs in Fig.8 are the same as in Fig.6 demonstrating that the concurrent improvement of EH-TMDI motion control and energy harvesting performances for non-grounded inerter with increase of inertance is not compromised by the level of external forces correlation. In fact,

Giaralis A. An inerter-based dynamic vibration absorber with concurrently enhanced energy harvesting and motion control performances under broadband stochastic excitation via inertance amplification. *ASCE-ASME Journal of Risk and Uncertainty in Engineering Systems Part B: Mechanical Engineering, accepted*: 16/11/2020.

careful cross-inspection of the four panels between Figs. 6 and 8 shows that the rate of improvement of the two PIs with inertance are almost identical.

To examine further the influence of the external forces correlation, Fig. 9 plots the two PIs in Eq.(31) with inertance for μ_s=0.1, γ_s= 1 and for three different levels of external force correlation. It is observed that for any given inertance, the EH-TMDI vibration suppression performance increases as the correlation, ρ, of the external forces reduces. This trend is attributed to the higher level of engagement of the inerter as the externally applied forces become less correlated. However, the rate of change of vibration suppression performance with inertance is unaffected by the correlation of the external forces, that is, the curves in Fig.9(a) are practically parallel. On the antipode, energy harvesting potential improves significantly with inertance in Fig.9(b) (for β>5%) and the rate of improvement (i.e., the slope of the curves in Fig.9(b) for β>5%) does depend on the external forces correlation. Specifically, the rate is reduced for fully correlated external forces, ρ=1, compared to partially correlated forces, ρ=0.5. Consequently, the energy harvesting performance curves for ρ=0.5 and ρ=1 intersect. This, in turn, suggests that the relation between external forces correlation and energy harvesting potential depends on the inertance and is not always positive. For this particular numerical example, the energy harvesting potential reduces as external forces correlation increases from ρ=0.5 to ρ=1 for β>55%, while the opposite happens for β<55%. This is an important consideration in wind engineering applications since wind field forces are spatially correlated (see e.g., Petrini et al. 2020).

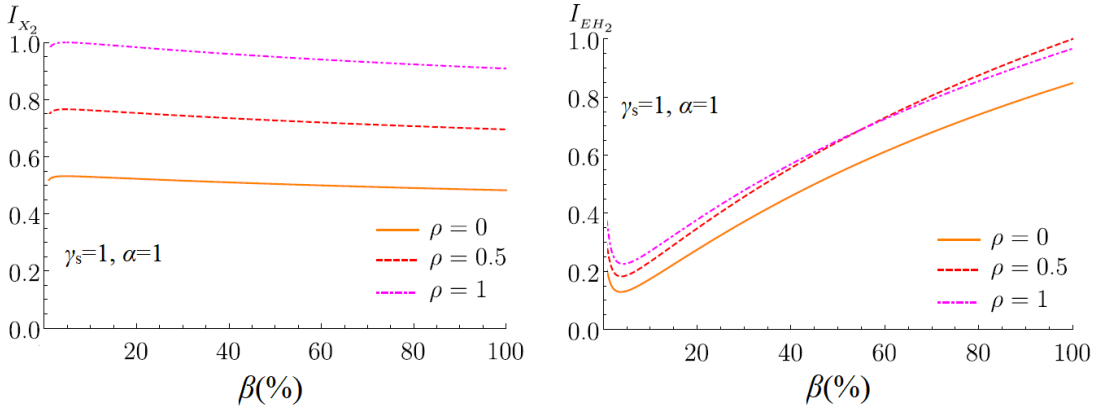

Figure 9. Motion control and energy harvesting performance indices in Eq. (33) normalized to their peak value for correlated (ρ=0.5) white noise force-excited EH-TMDI-equipped 2-DOF primary structures with various values of stiffness ratio γs, and with $\zeta_{s,1}$= $\zeta_{s,1}$=5%, ζ_{EH}= 10%, ζ_p=1%, μ_T= 1%, and μ_s=0.1, plotted against the inertance ratio β.

Collectively, the reported data demonstrate that, contrary to the case of EH-TMDI with grounded inerter, the vibration suppression performance of EH-TMDI with non-grounded inerter improves insignificantly with inertance scale up unless a sufficiently low stiffness ratio γ_s (i.e., flexible connection of the two primary structure masses) is adopted. In this regard, the primary structure softening has a positive influence to the EH-TMDI vibration suppression which is also the case for the TMDI (see Wang and Giaralis 2021). At the same time, EH-TMDI energy harvesting potential increases appreciably with inertance even for non-grounded inerter and primary structure flexibility benefits the rate of this increase with inertance. These observations lead to the fact that inertance scaling-up in the

Giaralis A. An inerter-based dynamic vibration absorber with concurrently enhanced energy harvesting and motion control performances under broadband stochastic excitation via inertance amplification. *ASCE-ASME Journal of Risk and Uncertainty in Engineering Systems Part B: Mechanical Engineering, accepted*: 16/11/2020.

EH-TMDI with non-grounded inerter can have similar beneficial effects to both vibration suppression and energy harvesting so long as the primary structure is judicially designed.

5. Concluding remarks

The potential of a regenerative inerter-based DVA, termed EH-TMDI, has been numerically assessed for the dual simultaneous objectives of vibration suppression and energy harvesting under increasing inertance in random white noise-excited linear damped primary structures. The cases of both SDOF and MDOF primary structures were considered. For application to SDOF primary structures, the EH-TMDI featured a grounded inerter and the parametric investigation focused on the influence of the system damping properties under force and base white noise excitations. In the case of MDOF primary structures, the inerter of the EH-TMDI is non-grounded and is engaged by the primary structure deformation under spatially correlated random white noise forces, thus the influence of the primary structure stiffness properties and the attributes of the random loading were considered in the parametric investigation.

For both types of primary structures, it was found that lightweight EH-TMDIs (attached mass less than 1% of the primary structure mass) performs better in terms of mitigating primary structure displacement and generating more energy as inertance is amplified in conjunction with simplified tuning of EH-TMDI stiffness and damping properties for undamped white noise excited primary structures. This is a practically important result since inertance is readily scalable, as seen in numerous recent prototyped inerter devices, while DVAs with small secondary mass are cost-effective and are easier to accommodate by new and existing primary structures. A further important finding is that the rate of improvement of vibration suppression and energy harvesting increases with inertance for more lightly damped primary structures and/or for increased energy harvesting damping ratio at the EM device. In this regard, accurate estimate of the inherent structural damping as well as detailed modelling of the energy harvesting circuitry become essential for the design and assessment of EH-TMDI performance in real-life applications. Both these considerations warrant further theoretical and experimental research work. Moreover, it was found that the performance of EH-TMDI with non-grounded inerter embedded within MDOF primary structures depends primarily on the stiffness distribution of the primary structure and less on the correlation and relative amplitude of the external random white noise. In particular, EH-TMDI performance improves significantly as inertance is amplified both in terms of vibration suppression and energy harvesting for primary structures with increased flexibility (lower stiffness) between the two locations that the EH-TMDI is attached to. The latter finding suggests that integrated design of the DVA with primary structure within a multi-objective optimization context is required to reach the full potential of the EH-TMDI. This consideration opens opportunities for further promising application-dependent future research work.

As a final remark, it is noted that all the herein reported trends and conclusions pertain to broadband/white stationary excitation and to linear models with ideal inerter element. In this respect, further research is warranted to assess the EH-TMDI configuration for case-specific narrowband and/or non-stationary excitations using appropriate indices to measure vibration suppression and energy harvesting performances as well as EH-TMDI tuning. Additional research is also required to gauge the effect of nonlinearities and non-ideal behavior related to the specifics of the energy harvesting and storage circuitry as well as of the inerter devices. Still, the facts that EH-TMDI motion control and energy harvesting performance increases with inertance for harmonic excitations (see Salvi and Giaralis

Giaralis A. An inerter-based dynamic vibration absorber with concurrently enhanced energy harvesting and motion control performances under broadband stochastic excitation via inertance amplification. *ASCE-ASME Journal of Risk and Uncertainty in Engineering Systems Part B: Mechanical Engineering, accepted*: 16/11/2020.

2016 and Appendix B), and that non-ideal inerter behaviour does not significantly compromise the performance of inerter-based DVAs (Gonzales-Buelga et al. 2017, Pietrosanti et al. 2020) suggest that favourable EH-TMDI performance with inertance amplification may be maintained for narrow-band random excitations and nonlinear system response upon tailored tuning.

Appendix A

The admittance matrix in Eq.(13) is expanded as

$$\mathbf{H}(g)=\frac{1}{\Delta}\begin{bmatrix} H_{11}(g) & H_{12}(g) & H_{13}(g) \\ H_{21}(g) & H_{22}(g) & H_{23}(g) \\ H_{31}(g) & H_{32}(g) & H_{33}(g) \end{bmatrix} \tag{A1}$$

where $\Delta=\det(-g^2\mathbf{M} + ig\mathbf{C} + \mathbf{K})$ and

$$\begin{aligned}
&H_{11}(g)=\left[-g^2\mu+2ig\left(\zeta_T+\zeta_{EM}\right)fM+f^2M\right]\left(-g^2\beta+2ig\zeta_{EM}\,fM\right)-\left(2g\zeta_{EM}\,fM\right)^2,\\
&H_{21}(g)=H_{12}(g)=\left(2ig\zeta_T\,fM+f^2M\right)\left(-g^2\beta+2ig\zeta_{EM}\,fM\right),\\
&H_{31}(g)=H_{13}(g)=2ig\zeta_{EM}\,fM\left(2ig\zeta_T\,fM+f^2M\right),\\
&H_{22}(g)=\left[-g^2+2ig\left(\zeta_s+\zeta_T\,fM\right)+\left(1+f^2M\right)\right]\left(-g^2\beta+2ig\zeta_{EM}\,fM\right),\\
&H_{32}(g)=H_{23}(g)=2ig\zeta_{EM}\,fM\left[-g^2+2ig\left(\zeta_s+\zeta_T\,fM\right)+\left(1+f^2M\right)\right],\\
&H_{33}(g)=\left[-g^2+2ig\left(\zeta_s+\zeta_T\,fM\right)+\left(1+f^2M\right)\right]+\left[-g^2\mu+2ig\left(\zeta_T+\zeta_{EM}\right)fM+f^2M\right]-\left(2ig\zeta_{EM}\,fM+f^2M\right)^2
\end{aligned} \tag{A2}$$

and $M=\mu+\beta$.

The elements of the impedance matrix in Eq.(30) are written as

$$\begin{aligned}
&Z_{11}(\tilde{g})=-g^2(1+\beta)+2i\tilde{g}\left(\zeta_{s,1}+\zeta_{s,2}f_s\mu_s\right)+1+f_s^2\mu_s,\\
&Z_{21}(\tilde{g})=Z_{12}(\tilde{g})=-2ig\zeta_{s,2}f_s\mu_s-f_s^2\mu_s,\\
&Z_{31}(\tilde{g})=Z_{13}(\tilde{g})=Z_{24}(\tilde{g})=Z_{42}(\tilde{g})=0,\quad Z_{41}(\tilde{g})=Z_{14}(\tilde{g})=\tilde{g}^2\beta,\\
&Z_{22}(\tilde{g})=-\tilde{g}^2\mu_s+2i\tilde{g}\left(\zeta_{s,2}f_s\mu_s+\zeta_T f_T M_T\right)+f_s^2\mu_s+f_T^2M_T,\\
&Z_{32}(\tilde{g})=Z_{23}(\tilde{g})=-2i\tilde{g}\zeta_T f_T M_T-f_T^2M_T,\\
&Z_{33}(\tilde{g})=-\tilde{g}^2\mu_T+2i\tilde{g}\left(\zeta_T+\zeta_{EM}\right)f_T M_T+f_T^2M_T,\\
&Z_{34}(\tilde{g})=Z_{43}(\tilde{g})=-2i\tilde{g}\zeta_{EM}f_T M_T,\quad Z_{44}(\tilde{g})=-\tilde{g}^2\beta+2i\tilde{g}\zeta_{EM}f_T M_T
\end{aligned} \tag{A3}$$

where $M_T=\mu_T+\beta$ and

$$f_s=\frac{\omega_{s,2}}{\omega_{s,1}}\quad\text{and}\quad f_T=\frac{\omega_T}{\omega_{s,1}}. \tag{A4}$$

Giaralis A. An inerter-based dynamic vibration absorber with concurrently enhanced energy harvesting and motion control performances under broadband stochastic excitation via inertance amplification. *ASCE-ASME Journal of Risk and Uncertainty in Engineering Systems Part B: Mechanical Engineering, accepted*: 16/11/2020.

Appendix B

This appendix presents numerical evidence to illustrate the unique attribute of the EH-TMDI configuration discussed in Section 2 and defined in Salvi and Giaralis (2016) to achieve concurrently improved vibration suppression and energy generation under resonant harmonic excitation (i.e., g=1) as inertance increases over alternative regenerative (energy harvesting capable) DVA configurations studied in the literature.

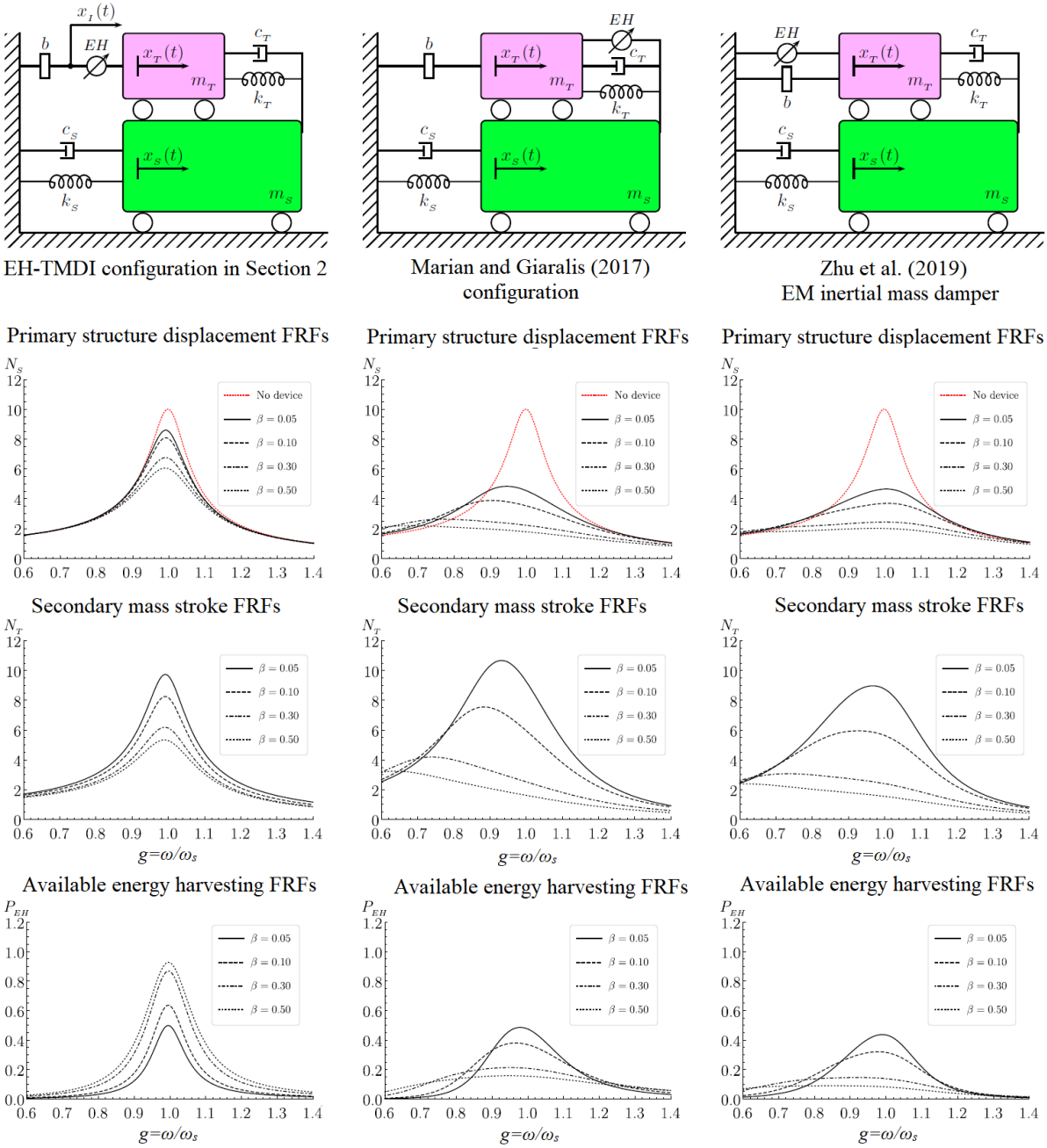

Figure B1. Mechanical models of damped SDOF primary structures equipped with three different regenerative DVAs with grounded inerter and corresponding dimensionless FRFs in terms of primary structure displacement, N_S, secondary mass displacement, N_T, and available energy for harvesting, P_{EH}, for inherent structural damping ratio ζ_s=5%, secondary mass ratio μ=1%, parasitic damping ratio ζ_p=1%, and energy harvesting ratio ζ_{EH}=10% and for various inertance ratios β.

Giaralis A. An inerter-based dynamic vibration absorber with concurrently enhanced energy harvesting and motion control performances under broadband stochastic excitation via inertance amplification. *ASCE-ASME Journal of Risk and Uncertainty in Engineering Systems Part B: Mechanical Engineering, accepted*: 16/11/2020.

For this purpose, Fig. A juxtaposes the FRFs of the EH-TMDI in Fig.2 for ζ_s= 5%, mass ratio μ=1%, parasitic damping ratio ζ_p=1%, and energy harvesting ratio ζ_{EH}=10% (first column of panels in Fig. B1) with the corresponding FRFs of two different regenerative DVAs with the same properties. Note that all three alternative configurations feature a grounded inerter and FRFs for the same set of inertance values are provided. The middle column of panels in Fig. A considers the case of a TMDI with grounded inerter where the EM is sandwiched between the secondary and the primary mass studied by Marian and Giaralis (2017). Note that this is the most widely considered placement of the EM in TMDs with no inerter used for energy harvesting (e.g., Tang and Zuo 2012a, Zuo and Tang 2013, Shen et al. 2018, 2019). Further, the right column of panels in Fig. B1 considers a conventional TMD coupled with a grounded regenerative inertial EM detailed in Zhu et al. 2019 (see also Joubaneh and Barry 2019). The FRF plots in Fig. B1 demonstrate that for at least for resonant harmonic excitation, the EH-TMDI is the only configuration in which an increase of inertance yields improvement both in terms of vibration suppression (reduction to primary and secondary mass displacement amplitude) and energy harvesting potential (increase of P_{EH} FRF ordinates around resonant excitation).

Acknowledgements

This work has been partially funded by EPSRC in UK, under grant EP/M017621/1. The Author gratefully acknowledges this financial support. The aid of Dr Jonathan Salvi in preparing the figures of the manuscript is also gratefully acknowledged.

References

Adhikari, S., Friswell, M.I., and Inman, D.J. (2009). "Piezoelectric energy harvesting from broadband random vibrations." *Smart Materials and Structures*, **18**(11), 115005.

Brzeski, P., Lazarek, M., and Perlikowski, P. (2017). "Experimental study of the novel tuned mass damper with inerter which enables changes of inertance." *Journal of Sound and Vibrations*, **404**, 47–57.

Cassidy, I.L., Scruggs, J.T., Behrens, S. and Gavin, H.P. (2011), "Design and experimental characterization of an electromagnetic transducer for large-scale vibratory energy harvesting applications", *Journal of Intelligent Material Systems and Structures*, **22**(17), 2009-2024.

Dai, J., Xu, Z.D., and Gai, P.P. (2019). "Tuned mass-damper-inerter control of wind-induced vibration of flexible structures based on inerter location." *Engineering Structures*, **199**(15), 109585.

De Angelis, M., Perno, S., and Reggio, A. (2012). "Dynamic response and optimal design of structures with large mass ratio TMD." *Earthquake Engineering and Structural Dynamics*, **41**(1), 41-60.

De Angelis, M., Giaralis, A., Petrini, F., and Pietrosanti, D. (2019). "Optimal tuning and assessment of inertial dampers with grounded inerter for vibration control of seismically excited base-isolated systems." *Engineering Structures*, **196**, 109250. DOI: 10.1016/j.engstruct.2019.05.091.

Den Hartog, J.P. (1956). *Mechanical Vibrations, fourth edition*, McGraw-Hill, New York.

Elias, A., and Matsagar, V. (2017). "Research developments in vibration control of structures using passive tuned mass dampers." *Annual Reviews in Control*, **44**, 129-156. DOI:10.1016/j.arcontrol.2017.09.015

Giaralis, A., and Petrini, F. (2017). "Wind-induced vibration mitigation in tall buildings using the tuned mass-damper-inerter (TMDI)." *Journal of Structural Engineering, ASCE*, **143**(9), 04017127.

Giaralis, A., and Taflanidis, A.A. (2018). "Optimal tuned mass-damper-inerter (TMDI) design for seismically excited MDOF structures with model uncertainties based on reliability criteria." *Structural Control and Health Monitoring*, **25**, e2082.

Green, P.L., Hendijanizadeh, M., Simeone, L., and Elliott, S.J. (2016). "Probabilistic modelling of a rotational energy harvester." *Journal of Intelligent Material Systems and Structures*, **27**(4), 528-536. DOI: 10.1177/1045389X15573343.

Gonzalez-Buelga, A., Clare, L.R., Cammarano, A., Neild, S.A., Burrow, S.G., and Inman, D.J. (2014). "An optimised tuned mass damper/harvester device." *Structural Control and Health Monitoring*, **21**(8), 1154–1169.

Gonzalez-Buelga, A., Clare, L., Neild, S., Jiang, J.Z., and Inman, D.J. (2015). "An electromagnetic inerter-based vibration suppression device." *Smart Materials and Structures*, **24**(5), 055015.

Gonzalez -Buelga, A., Lazar, I.F., Jiang, J.Z., Neild, S.A., and Inman, D.J. (2017). " Assessing the effect of nonlinearities on the performance of a tuned inerter damper." *Structural Control and Health Monitoring*, **24**(3):e1879.

Hu, Y., Chen, M.Z.Q., Xu, S. and Liu Y. (2016), "Semiactive inerter and its application in adaptive tuned vibration absorbers", *IEEE Transactions on Control Systems* Technology, DOI:10.1109/TCST.2016.2552460.

Joubaneh, E.F., and Barry O.R. (2019). "On the improvement of vibration mitigation and energy harvesting using electromagnetic vibration absorber-inerter: Exact H_2 optimization." *Journal of Vibrations and Acoustics*, **141**, 061007.

Lazar, IF, Neild, S.A., and Wagg, D.J. (2014). "Using an inerter-based device for structural vibration suppression." *Earthquake Engineering and Structural Dynamics*, **43**(8), 1129–1147.

Lazarek, M., Brezski, P., and Perlikowski P. (2019). "Design and modelling of the CVT for adjustable inerter." *Journal of the Franklin Institute*, **356**, 7611-7625.

Lee, D., and Taylor, D.P. (2001). "Viscous damper development and future trends." *The Structural Design of Tall* Buildings, **10**(5): 311–320.

Liu, X., Jiang, J.Z., Titurus, B., and Harrison, A. (2018). "Model identification methodology for fluid-based inerters." *Mechanical Systems and Signal Processing*, **106**, 479-494.

Luo, Y., Sun, H., Wang, X., Zuo, L., and Chen, C., 2017, "Wind Induced Vibration Control and Energy Harvesting of Electromagnetic Resonant Shunt Tuned Mass-Damper-Inerter for Building Structures," Shock and Vibration, 4180134.

Marian, L., and Giaralis, A. (2013). "Optimal design of inerter devices combined with TMDs for vibration control of buildings exposed to stochastic seismic excitations." *Proc. 11th International Conference on Structural Safety and Reliability for Integrating Structural Analysis, Risk and Reliability, ICOSSAR 2013,* New York, paper #137, 1025-1032.

Marian, L., and Giaralis, A. (2014). "Optimal design of a novel tuned mass-damper-inerter (TMDI) passive vibration control configuration for stochastically support-excited structural systems." *Probabilistic Engineering Mechanics*, **38**:156–164.

Marian, L., and Giaralis, A. (2017). "The tuned mass-damper-inerter for harmonic vibrations suppression, attached mass reduction, and energy harvesting." *Smart Structures and Systems*, **19**(6), 665-678.

Palomera-Arias, R., Connor, J.J., and Ochsendorf, J.A. (2008). "Feasibility Study of Passive Electromagnetic Damping Systems." *Journal of Structural Engineering, ASCE*, **134**(1):164–170.

Giaralis A. An inerter-based dynamic vibration absorber with concurrently enhanced energy harvesting and motion control performances under broadband stochastic excitation via inertance amplification. *ASCE-ASME Journal of Risk and Uncertainty in Engineering Systems Part B: Mechanical Engineering, accepted*: 16/11/2020.

Papageorgiou, C., and Smith, M.C. (2005). "Laboratory experimental testing of Inerters." *Proc 44th IEEE Conference on Decision and Control and European Control Conference*, Seville, DOI: 10.1109/CDC.2005.1582679.

Petrini, F., Giaralis, A., and Wang, Z. (2020). "Optimal tuned mass-damper-inerter (TMDI) design in wind-excited tall buildings for occupants' comfort serviceability performance and energy harvesting." *Engineering Structures*, 204:109904. DOI: 10.1016/j.engstruct.2019.109904.

Pietrosanti, D., De Angelis, M., and Giaralis, A. (2020). "Experimental shaking table study of nonlinear SDOF system equipped with tuned mass damper inerter (TMDI) under harmonic excitation." *International Journal of Mechanical Sciences*, **184**, 105762.

Pietrosanti, D., De Angelis, M., Basili, M. (2020) "A generalized 2-DOF model for optimal design of MDOF structures controlled by Tuned Mass Damper Inerter (TMDI)" *International Journal of Mechanical Sciences*, **185**, 105849.

Salvi, J., and Giaralis, A. (2016). "Concept study of a novel energy harvesting-enabled tuned mass damper-inerter (EH-TMDI) device for vibration control of harmonically-excited structures." *Proc. 13th International Conference on Motion and Vibration Control, MOVIC 2016, Journal of Physics: Conference Series* 744, 012082, DOI: 10.1088/1742-6596/744/1/012082.

Sarkar, R., and Fitzgerald, B. (2020). "Vibration control of spar-type floating offshore wind turbine towers using a tuned mass-damper-inerter." *Structural Control and Health Monitoring*, **27**, e2471.

Shen, W., Zhu, S., Xu, Y-L., and Zhu, H-P. (2018). "Energy regenerative tuned mass dampers in high-rise buildings." *Structural Control and Health Monitoring*, **25**(1), e2072.

Shen, W., Zhu, S., and Zhu, H. (2019). "Unify energy harvesting and vibration control functions in randomly excited structures with electromagnetic devices." *Journal of Engineering Mechanics, ASCE*, **145**(1): 04018115. DOI: 10.1061/(ASCE) EM.1943-7889.0001548.

Smith, M.C. (2002). "Synthesis of Mechanical Networks: the Inerter." *IEEE Transactions on Automatic Control*, **47**(10), 1648– 1662.

Smith, M.C. (2020). "The inerter: a retrospective." *Annual Review of Control, Robotics, and Autonomous Systems*, **3**, 361–391.

Swift, S.J., Smith, M.C., Glover, A.R., Papageorgiou, C., Gartner, B., and Houghton, N.E. (2013). "Design and modelling of a fluid inerter." *International Journal of Control*, **86**(11), 2035-2051.

Tang, X., and Zuo, L. (2012). "Vibration energy harvesting from random force and motion excitations." *Smart Materials and Structures*, **21**(7), 075025.

Wang, F.C., Hong, M.F., and Lin, T.C. (2011) "Designing and testing a hydraulic inerter." *Proceedings of the Institution of Mechanical Engineers, Part C: Journal of Mechanical Engineering Science*, **225**(1), 66-72.

Wang, Z., and Giaralis, A. (2021). "Top-storey softening for enhanced mitigation of vortex shedding induced vibrations in wind-excited optimal tuned mass damper inerter (TMDI)-equipped tall buildings." *Journal of Structural Engineering, ASCE*, 147(1): 10.1061/(ASCE)ST.1943-541X.0002838.

Warburton, G.B. (1982). "Optimum absorber parameters for various combinations of response and excitation parameters." *Earthquake Engineering and Structural Dynamics*, **10**(3), 381–401.

Zhu, S., Shen, W.A., and Xu, Y-L. (2012). "Linear electromagnetic devices for vibration damping and energy harvesting: modeling and testing." *Engineering Structures*, **34**:198–212.

Zhu, H., Li, Y., Shen, W., and Zhu, S. (2019). "Mechanical and energy-harvesting model for electromagnetic inertial mass dampers." *Mechanical Systems and Signal Processing*, **120**, 203–220.

Giaralis A. An inerter-based dynamic vibration absorber with concurrently enhanced energy harvesting and motion control performances under broadband stochastic excitation via inertance amplification. *ASCE-ASME Journal of Risk and Uncertainty in Engineering Systems Part B: Mechanical Engineering, accepted*: 16/11/2020.

Zuo, L., and Cui, W. (2013). "Dual-functional energy-harvesting and vibration control: electromagnetic resonant shunt series tuned mass dampers." *Journal of Vibration and Acoustics, ASME*, **135**: 051018. DOI: 10.1115/1.4024095.

Zuo, L., and Tang, X. (2013). "Large-scale vibration energy harvesting." *Journal of Intelligent Materials Systems and Structures*, 24(11):1405–1430, 2013.